Comptes Rendus

Géoscience

Sciences de la Planète

Julie Tugend, Geoffroy Mohn, Thibault Duretz, Benoit Petri
and Laetitia Le Pourhiet

Extension of continental lithosphere in rifted margins: a review of thinning mechanisms

Review article

Geodynamics of Continents and Oceans – A tribute to Jean Aubouin

Extension of continental lithosphere in rifted margins: a review of thinning mechanisms

Julie Tugend [®],[*],[a]**, Geoffroy Mohn** [®],[a]**, Thibault Duretz** [®],[b]**, Benoit Petri** [®],[c] **and Laetitia Le Pourhiet** [®],[d]

[a] Laboratoire Géosciences et Environnement Cergy (GEC), CY Cergy Paris Université, 95000 Neuville sur Oise, France

[b] Institut für Geowissenschaften, Goethe-Universität Frankfurt, Frankfurt, Germany

[c] Institut Terre et Environnement de Strasbourg, Université de Strasbourg, CNRS, UMR7063, F-67084 Strasbourg, France

[d] Institut des Sciences de la Terre Paris, ISTeP UMR 7193, Sorbonne Université, CNRS-INSU, 75005 Paris, France

Current address: Commission for the Geological Map of the World, Paris, France (J. Tugend)

E-mail: julie.tugend@gmail.com (J. Tugend)

Abstract. Crustal geometries imaged at rifted margins show contrasted first-order morphologies (wide and narrow, symmetric or asymmetric conjugates). This contribution aims to review the mechanisms of continental lithospheric thinning and types of extensional structures that control the formation of rifted margins. We illustrate, using a two-layer numerical model (one for the crust and one for the mantle), how different modes of lithospheric thinning shape the end-member crustal geometries of rifted margins depending on the initial thermal conditions and extension rates. As already known, the activation of narrow or wide modes of lithospheric thinning depends on the rheological behaviour of the lower crust and its efficiency as a decoupling layer. Morphologies generated by narrow litho-spheric thinning modes compare well with Atlantic-type rifted margins (e.g., Iberia–Newfoundland) while wide lithospheric thinning modes better apply to marginal seas characterized by higher initial geothermal gradients (e.g., South China Sea). Finally, we also emphasize that continental lithosphere thinning is depth-dependent, part of which is transient and cannot easily be measured in natural systems.

Keywords. Lithosphere thinning, Rifted margins, Depth dependent thinning.

Manuscript received 31 July 2023, accepted 25 March 2024.

1. Introduction

Continental lithospheric thinning is a fundamental process of plate tectonics associated with the formation of sedimentary basins in various geodynamic settings including intracontinental rifts and rifted margins, as well as back-arc domains and post-orogenic contexts [see review in Cloetingh et al., 2013]. Continental lithosphere thinning can be triggered by several mechanisms such as tectonic extension, thermal thinning (active mantle upwelling), and mantle lithosphere delamination and is, hence, not limited to divergent settings. In this contribution, we offer a synthetic review of some key conceptual

---

[*] Corresponding author

models that shifted our understanding of the deformation modes and mechanisms of continental lithosphere thinning.

The tectonic and thermal thinning of the continental lithosphere are recorded in passive margins during rifting associated with the necking and breakup of the continental lithosphere. Lithospheric necking is a mechanical shear instability that occurs in extension [Braun and Beaumont, 1987, Brun, 1999, Brun and Beslier, 1996, Schmalholz and Mancktelow, 2016, Chenin et al., 2018]. In multi-layered rheological systems like the continental lithosphere, multiple levels of necking and associated isostatic adjustments modulate its record in sedimentary basins [Brun and Beslier, 1996, Cloetingh et al., 2013, Duretz et al., 2016]. The thinning of the continental lithosphere is achieved during lithospheric breakup, during which continental extension evolves into the localized accretion of oceanic lithosphere [Dewey and Bird, 1970, Falvey, 1974, Heezen, 1960, McKenzie, 1978, Whitmarsh et al., 2001]. Rifted margins have been and still are key natural laboratories to answer fundamental questions related to continental lithosphere thinning such as (1) where and how does the continental lithosphere thin? (2) what are the deformation modes and mechanisms of lithosphere thinning?

First kinematic models implying uniform stretching and thinning of the lithosphere during tectonic extension [e.g., McKenzie, 1978] have been challenged over the years by the improvement of seismic imaging techniques and other geophysical quantitative analyses in present-day rifted margins and the study of field analogues in mountain belts.

The quantification of extension and thinning from seismic data showed that the amount of extension measured from observed normal faulting is significantly less than that required to thin the whole crust or lithosphere [Reston, 2007a, Kusznir and Karner, 2007, for reviews]. This so-called "extension discrepancy" is now recognized in many rifted margins worldwide including the Iberia–Newfoundland margins, South China Sea, or Woodlark Basin [e.g., Davis and Kusznir, 2004]. Several explanations have been proposed to account for this extension discrepancy [e.g., see reviews in Davis and Kusznir, 2004, Reston, 2009]. One suggests that extension measured from normal faulting is largely underestimated because of sequential [Ranero and Pérez-Gussinyé,

2010] or unrecognized multiphase faulting [e.g., Reston, 2005, 2007a,b, Reston and McDermott, 2014]. Alternative explanations suggest that the extension and thinning of the whole crust and lithosphere exceed that accommodated by the brittle upper crust [Driscoll and Karner, 1998, Davis and Kusznir, 2004, Kusznir et al., 2005]. This mechanism is referred to as depth-dependent thinning (DDT) and implies that the thinning of the continental lithosphere is partitioned with depth.

The increasing acquisition of seismic surveys imaging rifted margins showed their diverse structural style and crustal structure [Figure 1; e.g., Reston, 2009, Clerc et al., 2018, Sapin et al., 2021]. This variability is generally interpreted as the result of different modes of deformation during extension [e.g., narrow or wide rifts, Buck, 1991], controlled by the initial conditions such as the geothermal gradient, the rheological stratification, or structural inheritance [e.g., Le Pourhiet et al., 2004, Duretz et al., 2016, Davis and Lavier, 2017, Tetreault and Buiter, 2018], erosion and sedimentation [Burov and Poliakov, 2001] and variable melt emplacement during rifting and breakup [e.g. White and McKenzie, 1989, Lu and Huismans, 2022]. The recognition of intra-crustal and intra-lithospheric deformation structures remains challenging solely based on seismic data. Intra-basement reflectors are more and more frequently imaged in seismic reflection data and have convincingly been interpreted as extensional intra-crustal shear zones [e.g., Fazlikhani et al., 2017, Clerc et al., 2015]. However, seismic reflectors correspond to the impedance contrasts related to variations in the physical properties of the rocks and their interpretation in terms of lithologies or deformation processes remains debatable.

Results from the (International) Ocean Drilling Program (I)ODP and Deep Sea Drilling Program (DSDP) combined to the study of onshore field analogues in mountain belts have been a game changer in the study of continental thinning mechanisms. On the one hand, direct access to rocks recording the deformation of the lithosphere showed the key role of large offset normal faults (i.e., detachment faults) and evidence for intra-crustal and intra-lithospheric shear zones. On the other hand, ODP legs provided evidence for subcontinental mantle exhumation in so-called Continent-Ocean Transition (COT) zones of the magma-poor Iberia–Newfoundland conjugate

margins [Boillot et al., 1987, Sawyer et al., 1994, Whitmarsh et al., 2001, Péron-Pinvidic et al., 2007, Welford et al., 2010]. Similar evidence for sub-continental mantle exhumation comes from the study of remnants of rifted margins preserved in the Alps and in the Pyrenees [Lemoine et al., 1987, Manatschal and Nievergelt, 1997, Desmurs et al., 2001, Lagabrielle and Bodinier, 2008, Jammes et al., 2009]. The presence of subcontinental mantle in the COT of so-called magma-poor rifted margins attests their non-uniform asynchronous extreme crustal and lithospheric mantle thinning.

These observations led to the development of an array of conceptual models aiming to explain continental lithosphere thinning mechanisms in rifts and rifted margins that are summarized hereafter. After an overview of the contrasted crustal geometries of rifted margins imaged by geophysical methods, we present a review of the main extensional structures identified in rifts and rifted margins. We then propose a thematic and historical perspective of the different mechanisms and deformation modes of continental lithosphere thinning. Finally, we illustrate how these deformation modes depend on different geotherms and extension rates using a set of simple numerical simulations of lithospheric extension. Results of these numerical simulations are then compared to natural examples, if they exist.

More generally, this review emphasizes the variability and complementarity in time and space of continental lithosphere thinning mechanisms during extension and their influence on the morphology of rifted margins.

2. Where does the continental lithosphere thin?

Continental rifted margins, in contrast to rift systems, record the complete thinning of the continental lithosphere and its rupture leading to stable oceanic lithosphere accretion. Thereby, they represent unique natural laboratories where the final product of continental lithosphere extension can be observed. Although the crustal structure of rifted margins can now be imaged at high resolution by geophysical methods (Figure 1) (e.g., seismic reflection and refraction, or gravity and magnetic modelling), their continental breakup occurred millions

of years ago, and they started recording or recorded post-rift lithosphere thermal cooling.

2.1. *Crustal structure of rifted continental margins*

Compilations of seismic images and geophysical models show the variable morphology of rifted margins (Figure 1) [e.g., Reston, 2009, Clerc et al., 2018, Sapin et al., 2021]. This diversity is commonly interpreted as the result of different modes of extension operating in the heterogeneous continental lithosphere. Thereby, the different width of rifted margins is commonly interpreted as the result of drastically different rheological layering of the continental lithosphere [Buck, 1991, Hopper and Buck, 1996, Huismans and Beaumont, 2011, Pérez-Gussinyé and Reston, 2001]. Narrow rifts are commonly interpreted as resulting from the necking of strong layers while the presence of weak lower crust favours lower crustal flow and de/re-localization of the deformation [Buck, 1991]. Contrasted crustal geometries are observed between rifted margin examples but also between conjugate profiles (Figure 1). Quantifications of crustal and lithosphere thinning mechanisms are therefore even more revealing if they are derived from the analysis of conjugate rifted margin profiles. For this reason, in our compilation, we present conjugate sets of passive margin examples derived from seismic refraction and gravity datasets (Figure 1).

The crustal structure of rifted margins (Figure 1) is shaped by thinning mechanisms during extension, but also depends on the volumes of magma emplaced before, during and after the breakup. The inferred amount of magmatism and its timing of emplacement and extrusion relative to crustal thinning have therefore been used to characterize passive margin morphologies [White and McKenzie, 1989, Tugend et al., 2020]. In the case of so-called magma-rich rifted margins (also referred to as volcanic margins) where large volumes of magmatic rocks intrude the continental lithosphere and/or where an early onset of magmatism occurs relative to continental crustal thinning [Tugend et al., 2020], the imaged crustal structure does not only result from thinning processes (Figure 1a/b). Hence, although magma-rich rifted margins also record lithosphere thinning,
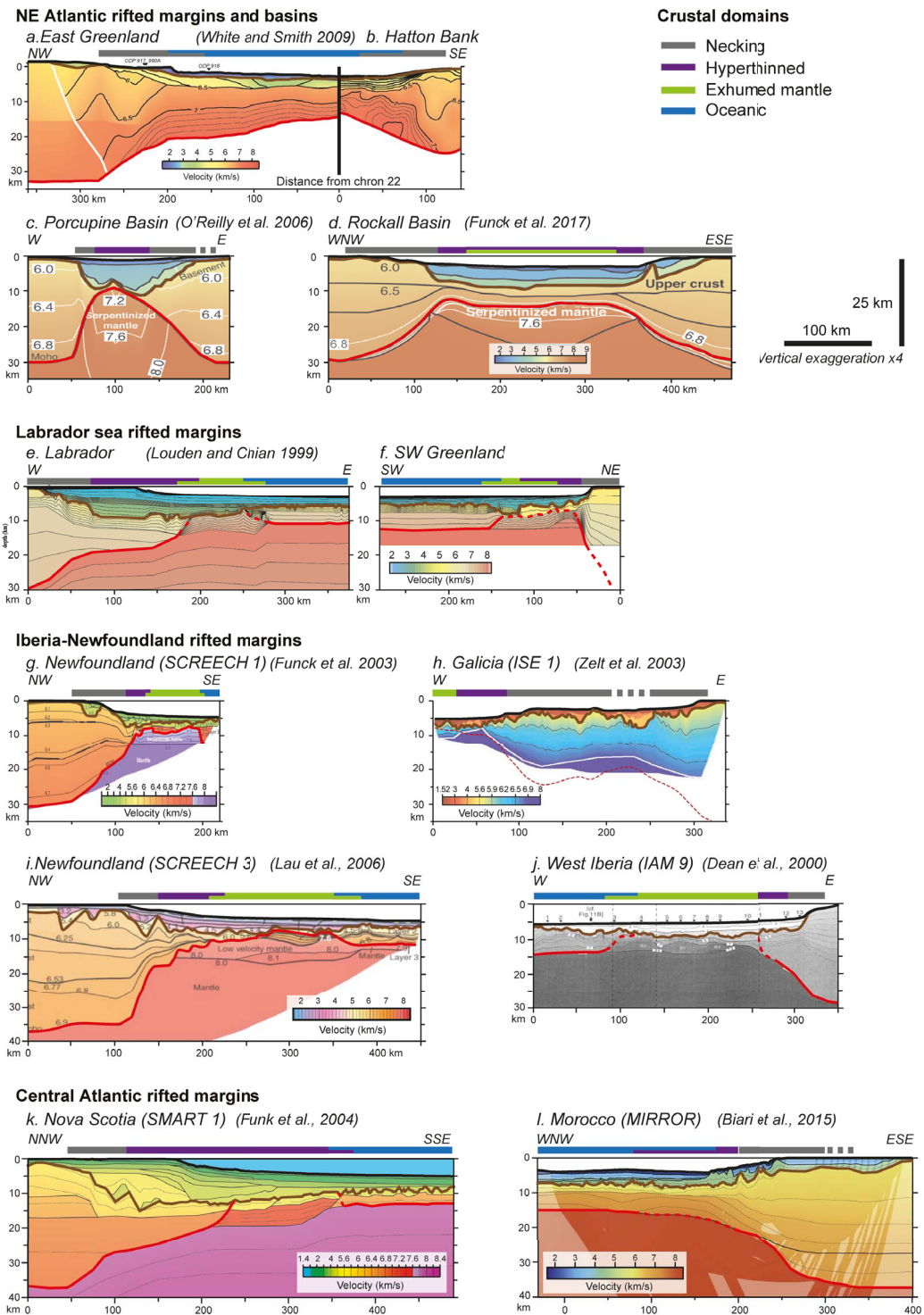
Figure 1. Continued on next page.

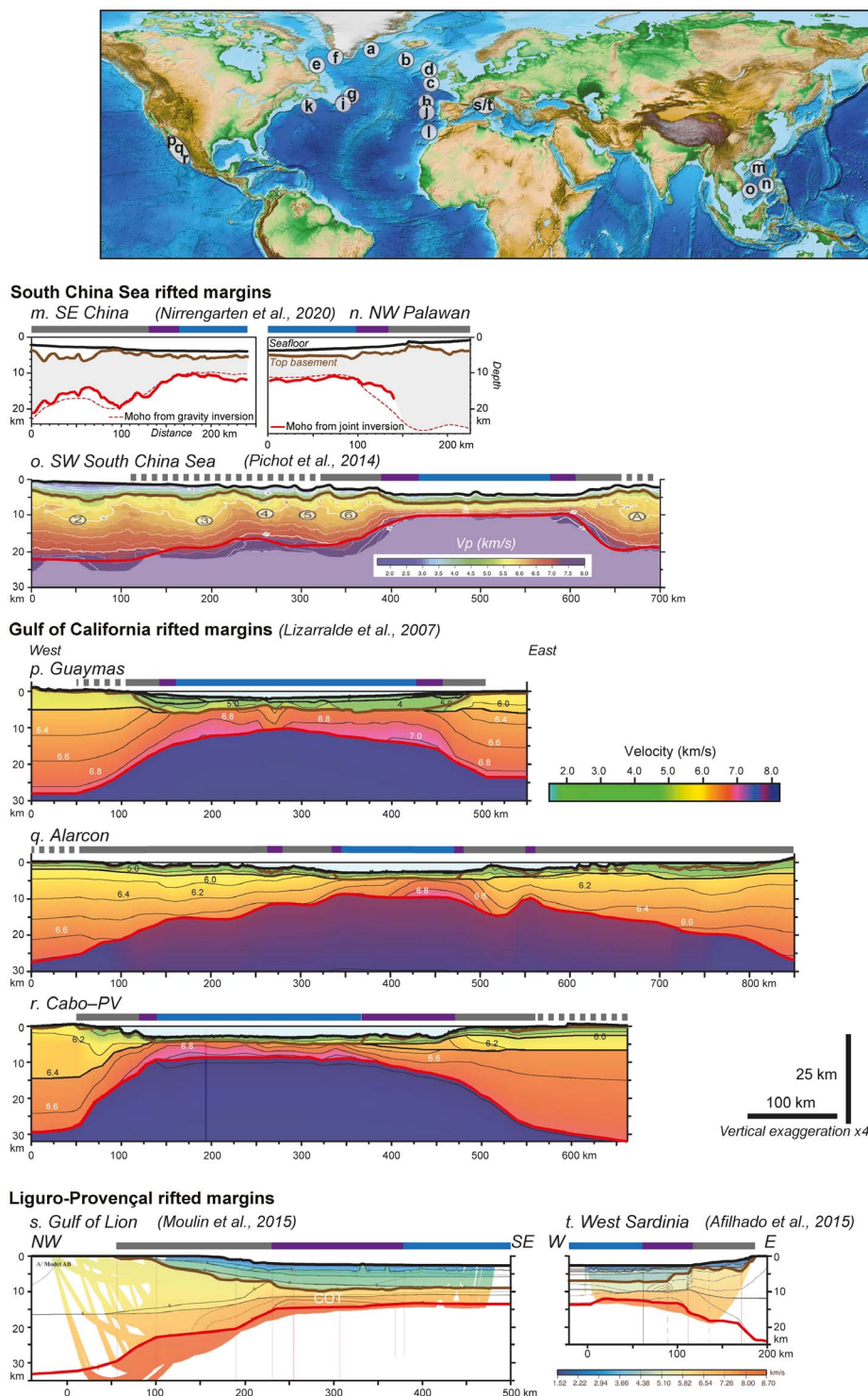**Figure 1 (cont.).** Crustal scale profiles across rift basins and conjugate rifted margins as imaged by refraction seismic data or modelled from gravity anomalies. This compilation shows the variable geometry of passive margin crustal structure and crustal domains. References are indicated above each profile, their location is indicated on the bathymetric map (after NOAA National Geophysical Data Center, 2009).

the mechanisms at play and quantifications of continental lithosphere thinning cannot always easily be investigated and are debated [e.g., Eldholm et al., 1995, Geoffroy et al., 2015]. Rifted margins that record extreme crustal thinning to 15–10 km thick or less prior to melt extraction [i.e., magma-poor rifted margins, Reston, 2009, Tugend et al., 2020; marginal basins, Larsen et al., 2018, Mohn et al., 2022] appear like the best examples to study and quantify lithosphere thinning mechanisms during rifting (Figure 1c–t). In such examples, the observed crustal structure more straightforwardly depends on the extensional deformation modes operating during rifting and breakup. Many passive margins record polyphase rifting events prior to breakup as a result of distinct periods of extension, each one possibly having a different direction of extension [Bellahsen et al., 2006, Leroy et al., 2012, Frizon de Lamotte et al., 2015]. In such cases, quantification of thinning mechanisms from rifted margin crustal structure can only be done if the amount of extension from each phase can be analyzed.

2.2. *Domains of crustal thinning*

Despite the obvious diversity of rifted margin geometries [Reston, 2009, Clerc et al., 2018, Sapin et al., 2021] (Figure 1) similar crustal domains can usually be identified corresponding to different magnitudes of crustal thinning (Figure 1).

Onset of significant crustal thinning from a ~35–30 km thick crust (i.e., pre-rift continental crust thicknesses) to a less than ~15–10 km thick crust is marked by a deepening of the top basement and rise of the Moho that shape a necking of the continental crust [Thinon et al., 2003, Osmundsen and Ebbing, 2008, Mohn et al., 2012, Peron-Pinvidic et al., 2013, Tugend et al., 2015, Nonn et al., 2017]. The crustal geometry of so-called necking zones or necking domains hence contrasts with the roughly parallel geometry of the top basement and Moho observed in proximal domains where only a little crustal thinning occurs. Onset of the deepening of the top basement and rise of the Moho may be spatially offset (e.g., Figure 1l/p/r), in which case, the complete length of the necking domain [i.e., taper length in Osmundsen and Redfield, 2011] is defined with uncertainties and can be underestimated.

Necking domains commonly extend over distances ranging from ~25 km (i.e., Porcupine basin, Figure 1c) to ~100 km (i.e., Moroccan rifted margin, Figure 1l; Rockall basin, Figure 1d) defining a relatively abrupt crustal neck [Mohn et al., 2012]. Crustal thinning can be more progressive or associated with a pinch-and-swell crustal structure of the rifted margin, also resulting in wider (up to ~200 km and in some cases more than 300 km wide) loosely defined necking domains (e.g., Galicia margin, Figure 1h; South China Sea rifted margins, Figure 1m–o; Alarcon segment of the Gulf of California, Figure 1q). The geometry of passive margin necking zones is thus extremely variable (Figure 1). Their style may vary along strike [e.g., Gulf of California rifted margins: Figure 1p–r; Norwegian margin: Osmundsen and Redfield, 2011]. Conjugate rifted margins and basins can have relatively symmetric (Figure 1d/i–j) or largely asymmetric crustal necks [e.g., Figure 1c/g–h/s–t; Parentis basin: Tugend et al., 2015].

Most of the rifted margin crustal thinning is accommodated in necking zones. However, many passive continental margins undergo a final crustal thinning (from ~10 km thick crust to 0) prior to oceanic lithosphere accretion, in usually loosely defined continent-ocean-transitions (COT). COT, where defined, are characterized by severely thinned continental crust (less than 15–10 km thick) that can be associated to windows of exhumed lithospheric mantle in-between the necking and oceanic domain (Figure 1). Domains of hyper-thinned continental crust [Tugend et al., 2014, 2015], also referred to as the neck area [Thinon et al., 2003], hyper-extended [Peron-Pinvidic et al., 2013] or coupled domain [Sutra et al., 2013] show a relatively parallel top basement and Moho geometry that progressively converges seaward to form a continental crustal wedge (Figure 1). Exhumed mantle domains are not systematically observed, in which case hyper-thinned crust is found adjacent to the oceanic crust in a sharp transition [e.g., Nirrengarten et al., 2020, Mohn et al., 2022] (Figure 1m/n/o/p/q). Evidence for exhumed mantle domains is usually indirectly constrained from geophysical criteria, in the absence of drilled or dredged mantle rocks as part of the top basement as recovered in the Iberia–Newfoundland [Boillot et al., 1980, 1987, Sawyer et al., 1994] or East Antarctica margins [McCarthy et al., 2020].

The width of COT shown by our compilation is variable (from ~20 km to ~250 km) [see also Chenin et al., 2017]. Where hyper-thinned or exhumed mantle domains can be distinguished, this diversity

seems mostly related to the variable width of the inferred exhumed mantle domain, while the width of the hyper-thinned domain is commonly narrow (~25–50 km wide) and rarely reaches ~100 km wide [Figure 1k/i/r; Gabon rifted margin: Clerc et al., 2018]. It is worth noting that the width of hyper-thinned and exhumed mantle domains and more generally of COT is not necessarily comparable between conjugate profiles, except perhaps in the case of marginal sea basins examples like the South China Sea (Figure 1m/n/o) or Guaymas and Alarcon segments of the Gulf of California (Figure 1p/q).

3. How does the continental lithosphere thin?

The diverse morphologies of rift basins and rifted margins (Figure 1) suggest that different deformation modes and mechanisms can operate to thin the continental lithosphere generating different geometries of extensional structures. By analysing the crustal structure imaged by geophysical methods (Figure 1) and exposed rift-related structures onshore, it is possible to quantify continental crustal thinning from the continent to the ocean and the role of the different types of extensional structures in accommodating lithosphere thinning.

3.1. *Extensional structures in rifted margins*

The thinning of the continental lithosphere is accommodated by an array of extensional structures with various geometries, active at different depths and periods of the rift evolution as well as rheological conditions. The recognition of extensional structures in present-day rifted margins is usually limited to those accommodating brittle deformation of the upper crust. Intra-basement reflectors are now also frequently identified thanks to the increasingly higher resolution of seismic reflection imaging techniques. Although convincing, their interpretation as extensional intra-crustal shear zones [e.g., Fazlikhani et al., 2017, Clerc et al., 2015] or in terms of lithologies or deformation process remains debatable. To lift these ambiguities, it is critical to complement these indirect observations with field observations either in onshore extensional systems [Jolivet et al., 2010, Fossen, 2010] or in fossil remnants preserved in orogenic systems [Handy and Zingg, 1991, Bissig and Hermann, 1999, Mohn et al., 2012, Petri et al., 2019]. In the latter case, the identification and description

of extensional structures rely on our capability to distinguish pre-orogenic (rift-related) from younger orogenic structures [Tugend et al., 2015, Mohn et al., 2022].

3.1.1. *High and low-angle normal faults*

Brittle extensional deformation of the uppermost basement is commonly accommodated by *high-angle normal faults* which control the formation of classical rift basins like horst and graben or half-graben in extensional settings. These extensional structures show either planar or listric geometries and are associated or not with block rotation. Each fault only accommodates a limited amount of lithosphere thinning. It should, however, be noted that many faults may be below the resolution of seismic imaging and hence accommodate more extension than that imaged in tilted blocks a situation referred to as distributed or subseismic faulting [Marrett and Allmendinger, 1992].

Nowadays, an increasing number of studies highlights the importance of *low-angle normal faults* (apparent dip <30–45°) in accommodating extensional deformation. Also often referred to as long offset normal faults [Brady et al., 2000], extensional detachments [Lister et al., 1986] or top basement detachment faults [Hölker et al., 2003], they can accommodate large displacements (>10s of kilometres) and exhume deep basement rocks in their footwall [Wernicke, 1981, Gautier et al., 1993, Jolivet et al., 2010, Whitney et al., 2013, Tugend et al., 2015]. Observations of low-angle normal faults active at <30° have triggered numerous debates. Their fault dip is lower than the 45–60° dip of normal faults predicted by fault mechanics [Anderson, 1951, see the review of Collettini, 2011]. For a long time, these structures were thought to result from the passive rotation of former high-angle normal faults that become inactive once their dip becomes significantly low (<30°). This rolling hinge model, notably proposed by Buck [1988], or Wernicke and Axen [1988] based on field evidence, has been successfully modelled [Brun et al., 1994, Lavier et al., 1999]. However, the existence of low-angle active normal faults in the Gulf of Corinth [Rigo et al., 1996] or in the Woodlark basin [Abers, 2001] remains enigmatic. Several hypotheses have been proposed to explain normal faults active and even formed at a low-angle including, stress rotation [Melosh, 1990], phyllosilicate

formation at the brittle–ductile transition [Gueydan et al., 2001], the reactivation of dipping lithological heterogeneities in a nappe stack [Le Pourhiet et al., 2004, Huet et al., 2011b] or their neoformation formation under a compaction regime [Lecomte et al., 2011, 2012].

Both models for the formation of low-angle normal faults (i.e., rolling hinge vs. detachment) are supported by observations in rifts and rifted margins but their involvement in accommodating continental lithosphere thinning may differ from one extensional system to the other. The formation of necking zones (Figure 1) has been associated with the development of long-offset low-angle normal faults, exhumation of continental basement and crustal thinning in many rifted margin examples [e.g., Osmundsen and Ebbing, 2008, Mohn et al., 2012, Tugend et al., 2015, Gresseth et al., 2023]. Top basement detachment faults are also commonly described in magma-poor COTs of rifted margins, where they are associated with the exhumation of lower crustal rocks and lithospheric mantle, after complete embrittlement of the continental crust [Pérez-Gussinyé and Reston, 2001]. The presence of such structures is confirmed by IODP drilling results in the Iberia–Newfoundland margins [Manatschal et al., 2001] and from field observations in the Alps [Lemoine et al., 1987, Froitzheim and Eberli, 1990, Manatschal, 2004] or Pyrenees [Jammes et al., 2009, Lagabrielle et al., 2019]. In marginal seas, low-angle normal faults commonly form core complex geometries associated with the exhumation of deep crustal rocks and emplacement of syn-kinematic magmatism [Woodlark Basin and Papua New Guinea: Abers, 2001; Thailand: Morley, 2014; South China Sea: Deng et al., 2020]. They are not necessarily associated with localized crustal thinning, in which case they are observed in diffuse necking zones (South China Sea rifted margin, Figure 1m/n/o). Normal faults active at low angle are also present in COTs of marginal seas where they have been shown to control the latest stage of continental breakup [Mohn et al., 2022; Woodlark Basin: Taylor and Huchon, 2002]. The geodynamic setting of marginal seas, including a high geothermal gradient, fast extension rate, and numerous inherited thrust faults seems to favour the formation of low-angle normal faults in the continental basement [Mohn et al., 2022]. Specifically, the occurrence of former nappe stacks may enhance the development

of such structures [Le Pourhiet et al., 2004, Huet et al., 2011b].

3.1.2. *Ductile extensional shear zones*

In contrast, the identification and interpretation of extensional structures accommodating continental lithosphere thinning at depth remain more problematic. Despite the increasing resolution of seismic reflection images, such structures are not easily observed, and their interpretation remains ambiguous. Below the brittle upper crust, extensional deformation has been interpreted as accommodated by ductile deformation, possibly associated with lower crustal flow [Buck, 1991] or localized along sets of extensional shear zones [Reston, 1988, Brun and Beslier, 1996, Huet et al., 2011a,b].

Extensional shear zones in the crust and the mantle that localize strain during continental lithosphere thinning have been identified and described in several fossil rifted margins sampled in mountain belts such as the Alps [Bissig and Hermann, 1999, Mohn et al., 2012, Kaczmarek and Müntener, 2008], Pyrenees [Aumar et al., 2022, Odlum et al., 2019], and the Betic-Rif belt [Gueydan et al., 2015, Frasca et al., 2016, Bessière et al., 2021]. Field observations show high- to low-angle ductile shear zones active in amphibolite to greenschist facies conditions accommodating the exhumation and juxtaposition of different levels of the continental lithosphere [Bissig and Hermann, 1999, Mohn et al., 2012, Frasca et al., 2016, Petri et al., 2019]. Some of these shear zones show low- to high-angle dips while others are sub-horizontal and are therefore interpreted as décollements. This association of low- to high-angle dipping shear zones and sub-horizontal décollements can lead to a heterogeneous thinning. This can result in the omission of specific layers of the continental lithosphere and juxtaposition of the upper crust against serpentinized mantle or lower crust for example [Frasca et al., 2016, Petri et al., 2019]. Such a process has been interpreted by Petri et al. [2019] as related to extraction tectonics that accommodate the thinning of continental lithosphere from the necking to the hyper-thinned domain.

Extensional mantle shear zones have also been identified in the upper mantle in former COTs preserved in the Alps [Lanzo massif: Kaczmarek and Müntener, 2008, Kaczmarek and Tommasi, 2011] or the Betic-Rif belt [Ronda or Beni Bousera massifs:

Afiri et al., 2011, Précigout et al., 2013, Gueydan et al., 2015]. These shear zones have been compared to possible analogous structures observed on seismic reflection data in present-day rifted margins [Gillard et al., 2019]. Field observations from these COTs report large scale, high-strain mantle shear zones that initiated at high temperature (approximately 1000 °C) and are interpreted to be active during the final rifting phase. These shear zones, as shown in the case of the Lanzo massif, can act as a permeability barrier below which mafic magma preferentially crystallize [Kaczmarek and Müntener, 2008].

3.2. *Measuring continental lithosphere thinning*

Spatial variations of the crust and lithosphere thicknesses define the geometry of rift basins and conjugate rifted margins and indicate how much stretching and thinning has been accommodated in the continental lithosphere during rifting. Strain can be measured from variations of rifted margin crustal structure in terms of a stretching (β) or thinning factor (γ) at the scale of the upper crust, whole crust, or whole lithosphere using different methods [see review in Davis and Kusznir, 2004].

The stretching factor can be measured in terms of horizontal extension (initial length is l_0 and length after extension is l):

$$\beta = \frac{l}{l_0}$$

The stretching factor can also commonly be defined as the ratio of the initial thickness of a layer (T_0) to the present-day thickness of that layer (T_{now}). Lithospheric thinning will eventually trigger decompression melting, resulting in the emplacement of magmatic additions and crustal thickening. If T_{ma} is the thickness of magmatic additions resulting from decompression melting, the stretching factor can be calculated as:

$$\beta = \frac{T_0}{T_{\text{now}} - T_{\text{ma}}}$$

The thinning factor is directly related to the stretching factor. It ranges from 0 (no thinning or extension) to 1 (infinite β value, i.e., complete thinning) and is often more convenient to represent graphically.

$$\gamma = 1 - \frac{1}{\beta}$$

The amount of brittle extension accommodated by the upper crust can be determined by measuring the horizontal displacement of faults interpreted in seismic profiles (fault heave summation method). Using this method, it is important to recognize low-angle top basement normal faults in seismic data to determine accurately the stretching factor derived from fault heave summation as pointed out by Gomez-Romeu et al. [2020]. Stretching and thinning factors for the whole crust can be determined if the crustal geometry down to the Moho can be imaged or modelled; the initial crustal thickness required in the calculation is typically inferred from adjacent unthinned regions. The magnitude of lithospheric thinning cannot be directly measured from the present-day lithosphere structure of passive margins as they at least partly recorded post-rift "thermal" subsidence [McKenzie, 1978]. Post-rift thermal subsidence as recorded in the stratigraphy of rifted margins can, however, be modelled in reverse to determine the whole lithosphere stretching or thinning following the method described in Roberts et al. [1998]. The calculation of these equivalent whole lithosphere stretching or thinning factors, however, assume that uniform stretching and thinning occurred [Davis and Kusznir, 2004].

3.3. *Mechanisms and deformation modes of continental lithosphere thinning*

Different conceptual models have been proposed to explain how the continental lithosphere thins during extension depending on the geometry of rift basins and type of extensional structures (Figure 2). They are either based on field observations [e.g., Wernicke and Axen, 1988, Lemoine et al., 1987, Manatschal, 2004, Mohn et al., 2012]; geophysical data [Reston, 1988, 2007a,b, Driscoll and Karner, 1998, Ranero and Pérez-Gussinyé, 2010], or analogue and numerical simulations [McKenzie, 1978, Brun and Beslier, 1996, Burov and Poliakov, 2001, Nagel and Buck, 2007, Lavier and Manatschal, 2006, Huismans and Beaumont, 2011].

Different mechanisms and deformation modes have been defined based on the initial conditions of the continental lithosphere, including crustal and lithospheric thickness, lithological or thermal structure, and structural inheritance [e.g., Ruppel, 1995]. Consequently, these mechanisms are dependent on
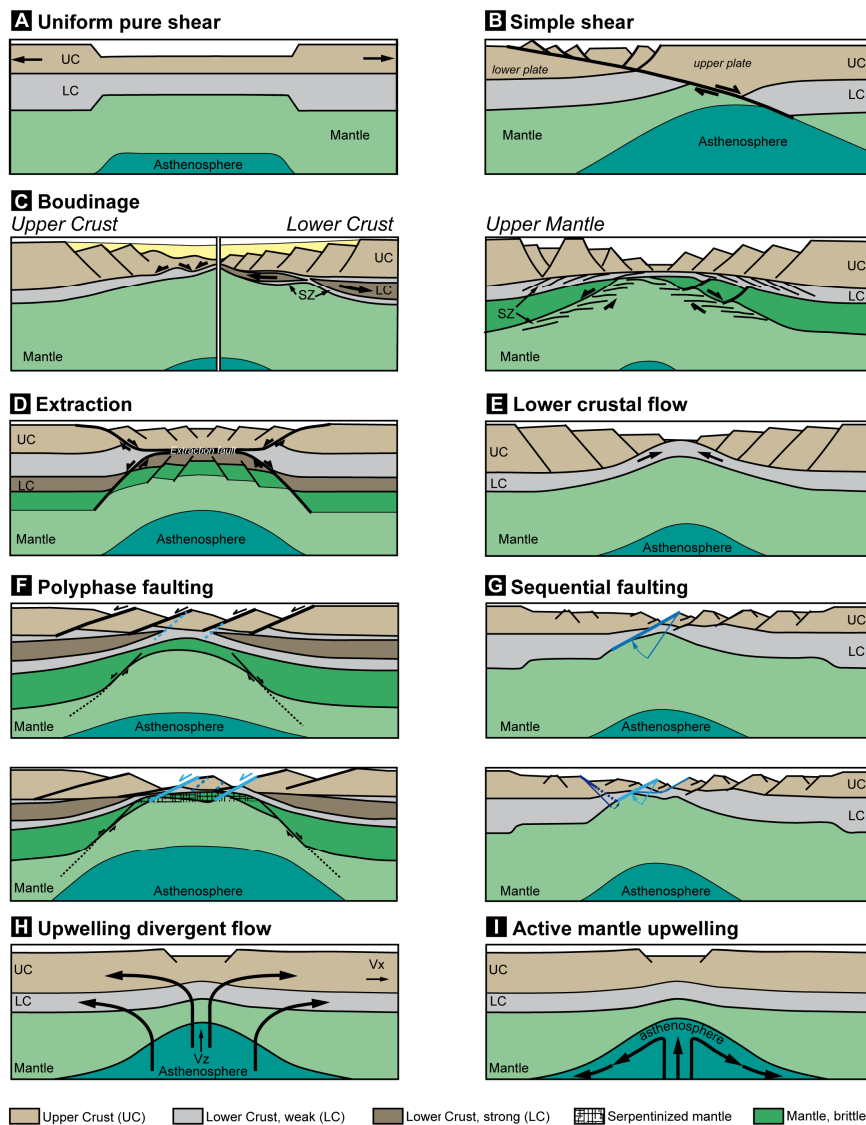
A **Uniform pure shear**

B **Simple shear**

C **Boudinage**
Upper Crust *Lower Crust*

Upper Mantle

D **Extraction**

E **Lower crustal flow**

F **Polyphase faulting**

G **Sequential faulting**

H **Upwelling divergent flow**

I **Active mantle upwelling**

Upper Crust (UC) | Lower Crust, weak (LC) | Lower Crust, strong (LC) | Serpentinized mantle | Mantle, brittle

Figure 2. Review of the main deformation modes and mechanisms of continental lithosphere thinning. (A) Uniform pure shear model [after McKenzie, 1978]; (B) Simple shear model [after Wernicke, 1995]; (C) Boudinage [upper crust after Clerc and Lagabrielle, 2014, lower crust after Reston, 1988; mantle after Brun and Beslier, 1996]; (D) Extraction [after Mohn et al., 2012]; (E) Lower crustal flow; (F) Polyphase faulting [after Reston, 2009]; (G) Sequential faulting [after Ranero and Pérez-Gussinyé, 2010]; (H) Upwelling divergent flow [after Kusznir and Karner, 2007]; (I) Active mantle upwelling [after Huismans et al., 2001].

the initial lithospheric rheological stratification. Because lithosphere rheology may evolve during rifting [Pérez-Gussinyé and Reston, 2001], a deformation mode can be activated during early or later rifting stages only and different thinning mechanisms can operate at different levels of the lithosphere.

3.3.1. *Uniform continental lithosphere thinning*

The first models assumed that the entire continental lithosphere is thinned by uniform pure shear extensional deformation (Figure 2A). This mechanism and its consequences for the thermal and

subsidence evolution of sedimentary basins were first quantified by McKenzie [1978]. The pure shear deformation model supposes a homogeneous thinning of the continental lithosphere by a stretching factor (β, see Section 3.2 for calculation methods). Instantaneous stretching and thinning of the continental lithosphere create space into which the asthenosphere passively rises. Crustal thinning results in subsidence while the passive rise of the asthenosphere generates a thermal uplift, the resultant of both effects being referred to as *initial subsidence or tectonic subsidence*. After thinning, the thermal perturbation of the lithosphere is predicted to cool conductively with time generating a slower phase of subsidence, the so-called *thermal subsidence*. It should be noted that in the initial uniform pure shear model of McKenzie [1978], the lithosphere is assumed to deform as a continuum rather than by faulting.

Despite its simplicity, the formulation of the pure shear model of McKenzie [1978] has been extensively applied to successfully predict the subsidence or heat flow evolution of intracontinental rift basins [e.g., the Gulf of Suez: Steckler et al., 1988; the Kenya Rift and the North Sea: Kusznir et al., 1995; the Jeanne d'Arc Basin: Kusznir, 1991]. This model is, however, unable to predict some of the observations made at distal rifted margins, including the presence of domains of exhumed mantle in some COT (Figure 1). As a result, its applicability to rifted margins recording an extreme thinning of the continental lithosphere has been widely discussed [see Davis and Kusznir, 2004, Kusznir and Karner, 2007, for reviews].

3.3.2. *Depth Dependent continental lithosphere Thinning (DDT)*

Extension and thinning have been measured extensively on the scale of the lithosphere, of the whole crust and of the upper crust (from fault heave summation) in many rifted margins worldwide [see review in Davis and Kusznir, 2004]. The results showed that the amount of extension that could be measured from brittle faulting in the upper crust was by far insufficient to balance the amount of thinning deduced at the scale of the whole crust or lithosphere [Davis and Kusznir, 2004, Reston, 2007a]. One explanation invoked for this identified "extension discrepancy" is that the thinning of the continental lithosphere is depth dependent: the different levels of the lithosphere (upper/lower crust and mantle) record differ-

ent magnitudes of thinning in space and time [see Reston, 2007a,b, Davis and Kusznir, 2004, Kusznir and Karner, 2007, Huismans and Beaumont, 2014, for reviews]. The concept of depth-dependent lithosphere stretching or depth-dependent lithosphere thinning (DDT) has been introduced in the 80s based on offshore [Eastern Canada margin, Royden and Keen, 1980] and onshore [Basin and Range, Wernicke, 1995] case studies. Over the past decades, numerous models involving DDT of the lithosphere have been proposed based on offshore and/or onshore datasets.

Non-uniform (decoupled) pure shear. The non-uniform pure shear model has initially been developed as an attempt to explain that quantifications of thermal subsidence were greater than predictions derived from crustal thinning only [Royden and Keen, 1980]. The non-uniform pure-shear deformation model is a variation of the McKenzie [1978] pure shear model, which incorporates the possibility of depth-dependent extension or thinning [Royden and Keen, 1980]. The non-uniform pure shear model considers that the lithosphere is constituted of layers with distinct mechanical behaviours that will not deform homogeneously under stress [e.g., Royden and Keen, 1980, Sclater and Christie, 1980]. As a result, different amounts of thinning are recorded above and below a decoupling horizon separating the brittle crust from ductile mantle; subsidence depends on the relative magnitude of thinning recorded by the two layers [Royden and Keen, 1980]. Despite its value to explain observations, this model implies that different amounts of extension are accommodated in the crust and mantle, which creates a problem to balance extension in 2D if the volume of mantle melt production is not considered [Royden and Keen, 1980].

Simple shear deformation model. An end-member of DDT is the simple-shear lithosphere extensional model [e.g., Wernicke, 1995, Wernicke and Axen, 1988, Lister et al., 1991] involving the activity of a major low-angle normal fault (i.e., detachment fault) cutting across the entire continental lithosphere (Figure 2B). This structure will produce two asymmetric margins with an upper and a lower plate. Extensional deformation will be nonuniformly distributed across the future rifted margins with a lateral shift between the location of extreme continental crust and lithospheric mantle thinning. This has implications

for both syn- and post-rift subsidence evolution between the upper and lower plates. However, the identification of upper and lower plates based on their subsidence evolution in mature systems has proven to be problematic due to important lower crust ductile extension and unrecognized normal faulting. Such a situation was referred to as the "upper plate paradox" by Driscoll and Karner [1998], implying that both margins appear as upper plates from their subsidence.

The simple-shear deformation model was invoked to explain the formation of several rifted margins such as the North Biscay margin [Le Pichon and Barbier, 1987] or the Alpine Tethys ones [Lemoine et al., 1987]. However, the original model implied that a low-angle normal fault can cut through the whole lithosphere, a situation that is plausible under extreme rheological conditions. The simple-shear deformation is commonly suggested to control the formation of some rifted margins but during the latest stage of rifting, once the crust is significantly thinned and embrittled [Pérez-Gussinyé and Reston, 2001, Manatschal et al., 2001].

Boudinage. The mechanical layering of the continental lithosphere is now commonly represented by at least four layers alternating strong (brittle) and weak (ductile) behaviours [Brun and Beslier, 1996]. Thinning of multi-layered lithosphere is not accommodated by either pure- or simple-shear deformation and generates a complex and heterogenous strain pattern.

Extension of a mechanically layered lithosphere triggers structural instabilities and softening accommodated by localized necking and boudinage of strong layers (Figure 2C/D) [Brun and Beslier, 1996, Mohn et al., 2012, Duretz et al., 2016, Clerc et al., 2018]. The disruption of competent layers is accommodated by shear zones acting as décollements in weak layers. Boudinage was initially inferred to occur in the deeper parts of the crust [Reston, 1988] and/or in the upper mantle [e.g., Brun and Beslier, 1996]. Boudinage of the upper crust was also suggested in examples inferred to have high thermal gradients and involving thick sedimentary layers [Clerc et al., 2018] or sediment/basement decoupling along salt layer [Clerc and Lagabrielle, 2014].

Extraction tectonics. In addition to the boudinage of strong layers, recent studies also highlighted the efficient role of extraction tectonics in accommodating continental lithosphere thinning based on field evidence and numerical simulations [Mohn et al., 2012, Duretz et al., 2016, Petri et al., 2019]. Extraction mechanisms occur in relation to the necking of competent layers. The necking or boudinage of strong layers results from strain localization along conjugate shear zones with opposite senses of displacement. With extension, strong layers will be coherently disrupted leaving behind an extraction fault or shear zone where most of the strain accumulated.

Extraction mechanisms appear critical during the necking of the heterogeneous lithosphere (Figure 1). Necking of the lithosphere results from the activity of conjugate large-offset normal faults interacting with anastomosing shear zones acting as décollement levels at mid-crustal levels or deeper (Figure 2D) [Mohn et al., 2012, Duretz et al., 2016, Petri et al., 2019]. During extension, weak ductile layers localize most of the deformation, resulting in vertical ductile thinning. Meanwhile, strong levels are laterally extracted towards the rift axis, forming the distal domains of rifted margins. As a result, distal domains predominantly retain strong levels and may preserve variable basement composition after extraction tectonics, depending on the initial heterogeneities [Petri et al., 2019].

DDT: the key role of the behaviour of the lower crust. At first order, the lower continental crust corresponds to the 10–17 km thick layer above the Moho. Although heterogenous and including various lithologies (felsic and/or mafic), it is often considered as a simple and uniform layer whose behaviour varies from strong, brittle or highly viscous [Jamtveit et al., 2016], to weakly viscous, in which case it can flow [Buck, 1991] and form a "channel flow" [Block and Royden, 1990, Huismans and Beaumont, 2011, Brune et al., 2014]. Geological models for the lower crust during rifting can be divided into two members depending on the non-flowing or flowing behaviour of the lower crust. The behaviour of the lower crust is directly related to the initial parameters of the rift system (e.g., thermal state, various inheritance) and can evolve during the development of extension through rheological softening mechanisms (temperature increase, occurrence of fluid/melt, grain size reduction along deformation zones).

On the one hand, the extension of the non-flowing lower crust is interpreted as being accommodated by a series of distributed shear zones. This mode of deformation was recognized on several reflection seismic profiles [Reston, 1988, Clerc et al., 2015], where reflective bands showing sigmoidal geometries were interpreted as localized shear zones accommodating lower crustal boudinage (Figure 2C). Additionally, it was confirmed through field observations in the Southern Alps, which preserve a section of lower crust from the former Jurassic Adriatic margin [Handy and Zingg, 1991, Mohn et al., 2012, Petri et al., 2019, Simonetti et al., 2021]. There, several synrift Jurassic shear zones delimit sections of Paleozoic basement unaffected by rift-related deformation.

On the other hand, several studies have emphasized the importance of lower crustal flow during extension [e.g., Block and Royden, 1990, Buck, 1991, Hopper and Buck, 1996, Huismans and Beaumont, 2011, Huet et al., 2011a, Brune et al., 2014]. Crustal thickness variations during thinning generate horizontal pressure gradients at the base of the crust. These pressure gradients can drive ductile lower crust, if its viscosity is sufficiently low, to flow into areas of localized upper crustal thinning (Figure 2D) [e.g., Artyushkov, 1973]. This mode of deformation initially referred to as the core complex mode by Buck [1991] involves a very weak lower crust so that the strain in the lower crust remains homogeneously distributed over a broad area. [Buck, 1991, Hopper and Buck, 1996]. Lower crustal flow is a mechanism commonly associated with the formation of metamorphic core complexes in post-orogenic settings [Whitney et al., 2013, and reference therein] or marginal basins [Gulf of Lion: Jolivet et al., 2015; South China: Deng et al., 2020] both of which are characterized by high-geothermal conditions.

3.3.3. *Extensional faulting*

Sequential faulting. Sequential faulting has been proposed as a solution to explain the extension discrepancy and asymmetry observed at some rifted margins (Figure 2E) [Ranero and Pérez-Gussinyé, 2010]. This deformation model is derived from observations in Iberia–Newfoundland rifted margins and suggests that crustal thinning is controlled by the activity of Andersonian-type extensional faults [Anderson, 1951]. Each fault locks after a rotation to >30° and is replaced by a new one formed in the

hanging wall of the locked fault. Consequently, each new fault forms in a previously thinned hanging wall, explaining why total crustal thinning exceeds that predicted by faulting at the same location, thus creating an apparent extension discrepancy.

Polyphase faulting. Alternative explanations for the "extensional discrepancy" observed at rifted margins suggest that the amount of extension measured from upper crustal brittle faulting is largely underestimated in seismic interpretations. Extension may notably go undetermined because of complex crosscutting relationships generated by polyphase faulting [Figure 2F, Reston, 2005, 2007a,b, 2009, Reston and McDermott, 2014]. This mechanism, derived from observations from the Iberia–Newfoundland rifted margins and introduced by Reston [2005] aims to explain the latest stages of thinning once the continental crust has become embrittled. Polyphase faulting contrasts with the sequential faulting mechanism and does not imply a migration, but rather a focusing of extensional deformation at the location of the future continental breakup. This mechanism implies successive phases of faulting: a first generation of fault forms, rotates to low angle and locks; then another generation of fault forms, cuts through the previous one, and so on. Complex fault intersections could then be generated and be difficult to identify on seismic profiles [Reston, 2005, 2007a,b, 2009, Reston and McDermott, 2014, Naliboff et al., 2017].

3.3.4. *Active upwelling*

Mantle dynamics can also play an active role during continental lithosphere thinning, which is often triggered by flow instabilities induced by viscosity contrasts, thermal and melt buoyancy forces (Figure 2H/I). The degree of active upwelling or buoyancy can be quantified by the ratio between extension (Vx) and axial upwelling rates (Vz) [Batchelor, 1967, Braun et al., 2000] as defined in the upwelling divergent flow model (Figure 2H) [Davis and Kusznir, 2004, Kusznir and Karner, 2007]. Upwelling divergent flow may be focused on the lower lithosphere, generating small-scale convection that contribute to thinning the mantle lithosphere (Figure 2I) [Huismans et al., 2001]. Dynamic models predict that small-scale convection in the mantle lithosphere can arise in the latest stages of rifting, inducing a transition from passive to active mantle upwelling [Huismans et al.,

2001]. Thermal anomalies in the mantle are particularly prone to triggering diapiric instabilities and small-scale convection in the asthenosphere [Nielsen and Hopper, 2004]. However, active upwelling is also a viable deformation mode in the absence of anomalously hot mantle [Davis and Kusznir, 2004, Kusznir and Karner, 2007, Fletcher et al., 2009, Jeanniot et al., 2016].

4. What are the parameters controlling the modes of continental lithosphere thinning?

Various mechanisms and deformation modes can operate to thin the continental lithosphere (Figure 2). Nevertheless, whether a deformation mode is activated or inhibited in lithospheric layers largely depends on the initial rheology and its evolution during rifting [Buck, 1991, Gueydan et al., 2008, Huismans and Beaumont, 2003, 2007, 2011, Huismans et al., 2005, Lavier and Buck, 2002]. Previous numerical studies have notably explored the role of parameters such as lithospheric strength and thermal structure, crustal thickness, structural inheritance or brittle–ductile mechanisms and extension rates on the modes of extension during rifting [Beaumont and Ings, 2012, Brune et al., 2014, 2017, Buck, 1991, Buck et al., 1999, Gueydan et al., 2008, Huismans et al., 2005, Huismans and Beaumont, 2007, 2011, Le Pourhiet et al., 2004, Jammes and Lavier, 2016, Svartman Dias et al., 2015, Tetreault and Buiter, 2018]. Most of these parameters and feedback between them also influence the final morphology of rifted margins (wide vs. narrow; symmetric vs. asymmetric). It would be beyond the scope of this review to do an exhaustive parametric study of all these parameters. Here, we built a set of numerical models only varying two key parameters to capture to first order the evolution of continental lithosphere thinning mechanisms over time within the different levels of the lithosphere.

4.1. *Modelling approach and initial configuration*

The presented numerical models were run using the 2D geodynamic simulation code MDoodz [Duretz et al., 2021]. The code is based on the finite-difference/marker-and-cell technique [Gerya and

Yuen, 2003] which allows to conveniently couple Eulerian thermomechanical numerical solutions with Lagrangian advection of material properties. The mechanical and thermal equations are discretized on a staggered grid and resulting linear systems are obtained via direct-iterative schemes [Räss et al., 2017]. Lagrangian markers are advected using a second order in space Runge–Kutta scheme. The models include a true free surface based on the staircase discretization and Lagrangian advection [Duretz et al., 2016]. Kinematic boundary conditions are applied to the left, right and bottom sides of the model domain.

The rheological model is visco-elastic–viscoplastic [de Borst and Duretz, 2020] (Table 1). The visco-elastic creep model includes the power-law effect of dislocation creep. Peierls and diffusion creep are additionally taken into account in mantle phases only. A Drucker–Prager frictional plastic model is applied to all material phases. The latter is supplemented by viscoplastic regularisation [Duretz et al., 2019], which allows for successful integration of the rheological models [Duretz et al., 2020]. At the local level, the rheology is integrated using local iterations [Popov and Sobolev, 2008]. At the global level, force equilibrium is achieved by applying Newton iterations [Duretz et al., 2021].

The model domain has a width of 350 km and a height of 170 km. The latter is discretized using to 910×500 cells, which provides a spatial resolution of 380 m along both dimensions. The domain extent remains fixed throughout the simulations. Material thus flows out of east and west boundaries and flows in from the south side. The crust has an initial thickness of 35 km and only consists of a single material phase (Westerly granite). The mantle also consists of a single material phase (dry olivine). In order to seed the model, an initial bell-shaped thermal perturbation is applied in the mantle (amplitude 50 °C and half-width 30 km). In the following, we investigate the role of two key parameters: the extension rate (0.25 to 2.3 cm/yr) and then Moho temperature (450 °C to 650 °C).

4.2. *Results of numerical simulations*

For each simulation, we show the initial strength profile and geotherm, the evolution of the crustal geometry and superimposed modes of deformation

Table 1. Thermal and rheological parameters used in the simulations

Lithology		Crust (Granite)	Mantle/Asthensphere (Olivine)	Units
ρ_0	Density	2800	3330	kg/m^3
n_{dis}	Stress exponent	3.3	3.5	
A_{dis}	Pre-exp factor	3.1623×10^{-26}	1.1×10^{-16}	Pa^{-n}·s^{-1}
Q_{dis}	Activation energy	185.5	530	kJ × mol^{-1}
V_{dis}	Activation volume	0	11×10^{-6}	m^3·mol^{-1}
n_{dif}	Stress exponent	-	1	
m_{dif}	Grain size exponent	-	3	
A_{dif}	Pre-exp. factor	-	1.5×10^{-15}	Pa^{-n}·m^m·s^{-1}
Q_{dif}	Activation energy	-	375	kJ·mol^{-1}
V_{dif}	Activation volume	-	4×10^{-6}	m^3·mol^{-1}
q_{pei}	Peierls parameter	-	2	
γ_{pei}	Peierls regularisation	-	0.1	
σ_{pei}	Peierls' stress	-	8.5	GPa
A_{pei}	Pre-exp. factor	-	5.7×10^{11}	s^{-1}
Q_{pei}	Activation energy	-	540	kJ·mol^{-1}

Flow law parameters are taken from Hansen and Carter [1983] for the crust, Hirth and Kohlstedt [2004] and Goetze and Evans [1979] for the lithospheric mantle with regularization from Kameyama et al. [1999]. The following parameters are similar for the crust and the mantle: Expansivity ($\alpha = 3.2 \times 10^{-5}$ K^{-1}), incompressibility ($\beta = 1.5 \times 10^{-11}$ Pa^{-1}), shear modulus ($G = 1.0 \times 10^{10}$ Pa), friction angle ($\varphi = 30°$), initial cohesion ($C_0 = 50$ MPa), final cohesion ($C_\infty = 1$ MPa), reference visco-elastic overstress ($\Delta\sigma = 1.5$ MPa), heat capacity ($C_p = 1050$ J/kg/K), thermal conductivity ($k = 3$ W/m/K). A grain size of 1 mm is assumed for the mantle. The governing equations and the detailed model implementation are stated in Duretz et al. [2021].

(distribution between elastic, plastic and viscous rheological behaviours) and strain distribution. Thinning factors for the crust, mantle and whole lithosphere are also shown to track the partitioning between the crust and lithospheric mantle thinning and evolution in space and time of DDT.

4.2.1. *Model NR01—cold Moho temperature and slow extension rate*

The model NR01 shown in the Figure 3 is characterized by an initial cold Moho temperature of 450 °C and a slow extension rate (0.25 cm/yr). The initial lithosphere–asthenosphere boundary (LAB) (1350 °C) is slightly deeper than 150 km depth (Figure 3a).

Extension is initially accommodated by discrete high-angle structures in the brittle/plastic upper part of the crust and mantle. Strain subsequently localizes at the rift axis in the uppermost brittle/plastic

mantle after 16% of the extension (Figure 3b). In the crust, strain starts localizing within two narrow conjugate deformation zones dipping toward the rift axis delimiting a central ~50 km wide graben. Although strain continues localizing within these conjugate deformation zones, the future necking zones, little brittle/plastic deformation is recorded in the central crustal block in between (Figure 3c) [so-called H-block: Lavier and Manatschal, 2006 or keystone: Mohn et al., 2012]. Increasing extension leads to the boudinage and distributed necking of the upper brittle/plastic mantle layer at the rift axis, accommodated by deformation of the ductile/viscous lower crust of the keystone that becomes heterogeneously thinned after 20% of extension. As increasing extension is accommodated within crustal conjugate deformation zones, increasing crustal thinning is being recorded in the forming necking zones associated with the exhumation and embrittlement of deeper
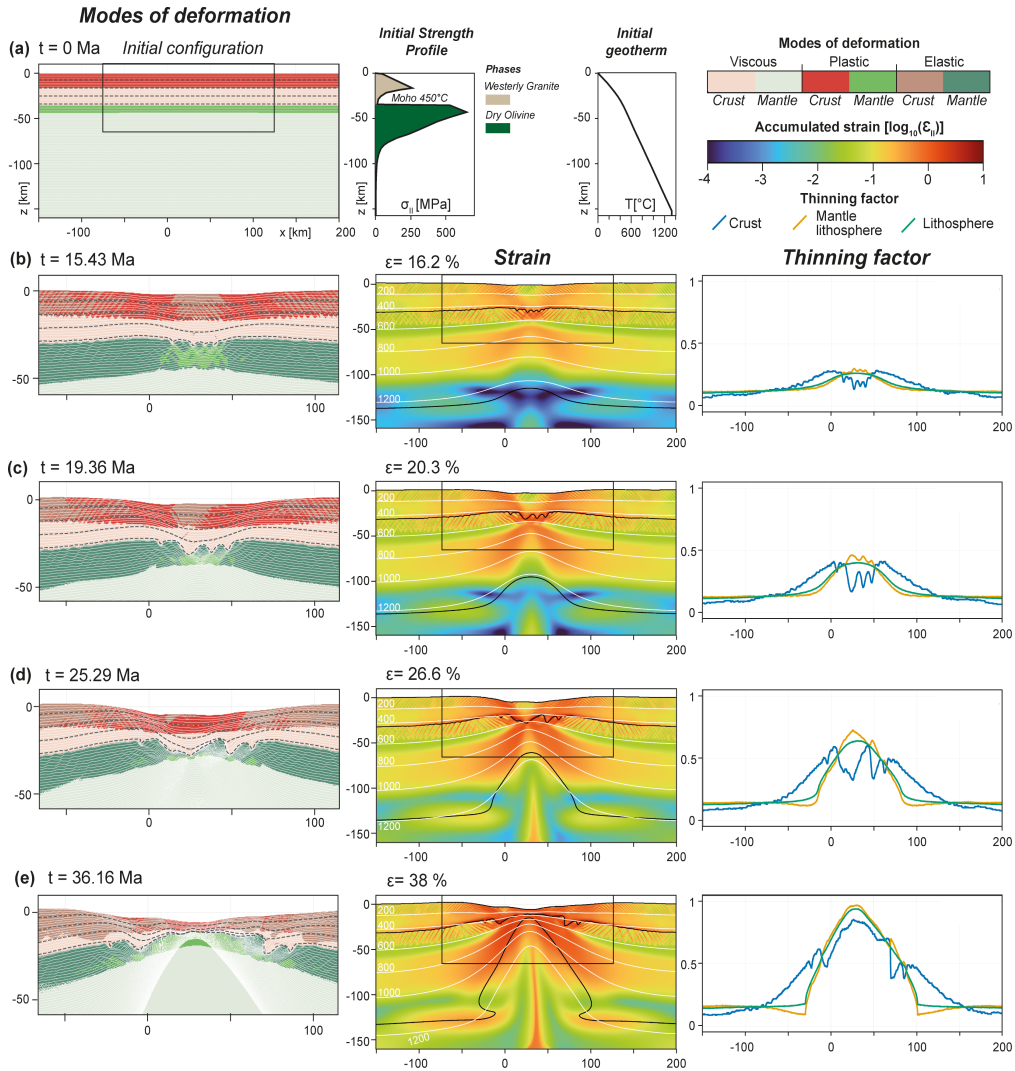
Figure 3. Numerical model NR01 illustrates the development of rifting with initial Moho temperature of 450 °C and a constant bulk extension rate of 0.333×10^{-15} s^{-1}. Left column represents an enlargement of the model showing the mode of deformations and their evolution during ongoing extension. The doted gray and thin white lines represent passive markers. Please note that the middle one represents the initial plastic elastic to viscous transition (i.e., brittle–ductile transition) The central column documents the accumulated von Mises strain (εII). The white contours show the isotherms in °C. The right column displays the thinning factor distribution across the model for the crust, the mantle lithosphere and the whole lithosphere.

crustal levels (see evolution of passive markers in Figure 3d). After 26% of extension, the deformation and thinning of the keystone crustal block intensifies, associated to transient asymmetric shearing. Crustal thinning of the keystone leads to its progressive embrittlement and thinning of ductile/viscous

lower crust (Figure 3e). After 38% of extension, only extremely thinned (<10 km) plastic/brittle crust remains in between the necking zones, underlain by a plastic/brittle upper mantle layer. Final crustal thinning and crustal separation is here accommodated in the frictional field (Figure 3e).

4.2.2. *Model NR03—cold Moho temperature and fast extension rate*

The model NR03 shown in Figure 4 is characterized by an initial cold Moho temperature (450 °C) and depth of the LAB similar to model NR01 (Figure 3) but with a larger extension rate (2.3 cm/yr) (Figure 4a).

Strain is initially accommodated by discrete distributed high-angle extensional faults in the brittle/plastic upper part of the crust and mantle. Similarly to model NR01, strain localizes in the brittle/plastic upper mantle at the rift axis at 17% of extension, associated to the formation of two deformation zones in the crust delimiting a central ~50 km wide graben (Figure 4b). Localized boudinage and necking of the brittle/plastic upper mantle layer occurs after 22% of extension, with a larger wavelength ductile/viscous deformation of the lower crust of the keystone compared to NR01 (Figure 4c). The forming necking zones already record intense crustal thinning ($\gamma \sim 0.5$ after 22% of extension, Figure 4c), while little brittle/plastic deformation of the keystone is recorded. Exhumation of deeper crustal levels and their embrittlement occur in the necking zones but are less pronounced than in model NR01. After 22% of extension, strain localizes in between the necking zones at the rift axis recorded by brittle/plastic deformation in the upper crust (Figure 4d). After 36% of extension, strain accumulation in the crust at the rift axis leads to the thinning and cutting of the central keystone block into symmetric parts (Figure 4e). Despite the extreme crustal thinning of the continental crust, it never fully embrittles before crustal separation (Figure 4e) in contrast to model NR01 (Figure 3e).

4.2.3. *Model NR07—hot Moho temperature and slow extension rate*

The model NR07 shown in Figure 5 is characterized by a higher temperature of 650 °C at the Moho and a low extension rate (0.25 cm/yr). The initial LAB (1350 °C) is slightly deeper than 90 km depth (Figure 5a).

Extension is accommodated by distributed discrete high-angle extensional faults in the brittle/plastic upper crust for 20 Ma. Strain subsequently localizes in the lithosphere towards the rift axis while active mantle upwelling is initiated at the base of the lithosphere. After 38% of extension, roughly homogeneous thinning is observed over a 200 km width at the rift axis although mantle thinning slightly exceeds crustal thinning (Figure 5b). Conductive cooling of the mantle due to the low extension rate enables the formation of a plastic/brittle upper mantle layer, subsequently thinned by short wavelength boudinage associated with ductile/viscous lower crust deformation (Figure 5b). A complex pattern of extensional structures occurs in the brittle/plastic upper crust, suggesting that several generations of faults formed (polyphase faulting) dipping in opposite directions. At 41% of extension, strain localizes in a narrower region at the rift axis, associated with the formation of two conjugate shear zones in the crust that delimit a central graben (up to 25 km wide), under which the crust is slightly thicker (Figure 5c). Extension and crustal thinning are accommodated by extensional shear zones within the necking zones, which are associated to the exhumation of deeper crustal levels (Figure 5d). Crustal thinning occurs beneath the central graben at the rift axis, associated with progressive crustal embrittlement from 44% to 49% extension (Figure 5e).

4.2.4. *Model NR09—hot Moho temperature and fast extension rate*

The model NR09 shown in Figure 6 is characterized by Moho temperature of 650 °C and depth of the LAB similar to model NR07 (Figure 5a), but with a faster extension rate (2.3 cm/yr) (Figure 6a).

During the first 10% of extension, the lithosphere records low-magnitude homogeneous thinning. As strain accumulates in the mantle, predominantly viscous deformation occurs within a roughly 150 km wide region at the rift axis, except for a thin (~2 km thick) plastic/brittle upper mantle layer. Simultaneously, multiple zones of brittle/plastic deformation develop in the upper crust due to its boudinage, while lower crustal domes gradually form between crustal boudins (Figure 6b). The large-scale boudinage of the upper crust persists until 30% of the extension, beyond which strain becomes localized at the rift axis within the mantle (Figure 6c). At this stage, several upper crustal boudins have formed recording brittle/plastic deformation, while deeper crustal levels are exhumed and embrittled in-between. As strain localizes at the rift axis, offset crustal deformation zones progressively deactivate
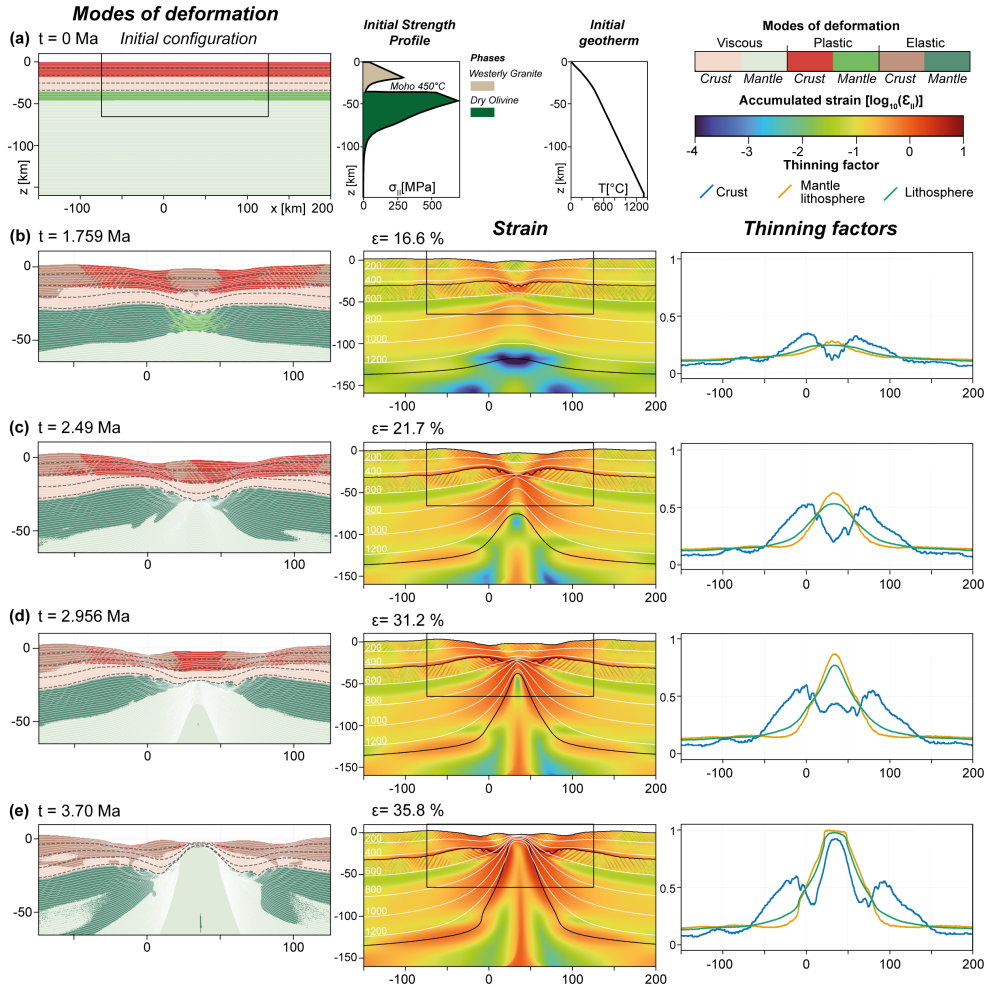
Figure 4. Numerical model NR03 illustrates the development of rifting with initial Moho temperature of 450 °C and a constant bulk extension rate of 3×10^{-15} s^{-1}. Left column represents an enlargement of the model showing the mode of deformations and their evolution during ongoing extension. The doted gray and thin white lines represent passive markers. Note that the middle one represents the initial plastic-elastic to viscous transition (i.e., brittle–ductile transition) The central column documents the accumulated von Mises strain (εII). The white contours show the isotherms in °C. The right column displays the thinning factor distribution across the model for the crust, the mantle lithosphere and the whole lithosphere.

after 30% of extension. Subsequently, strain localizes within one of these crustal deformation zones, nearest to the rift axis, resulting in asymmetric crustal thinning offset from the rift axis, with one of the crustal blocks ("boudins") preserved on one side (Figure 6d). After 37% extension, strain localization in the crust progressively shifts to localize above the rising asthenosphere, generating crustal scale simple-shear deformation. After 42% extension, extreme crustal thinning is recorded in the distal margin, without entailing complete crustal embrittlement (Figure 6e).
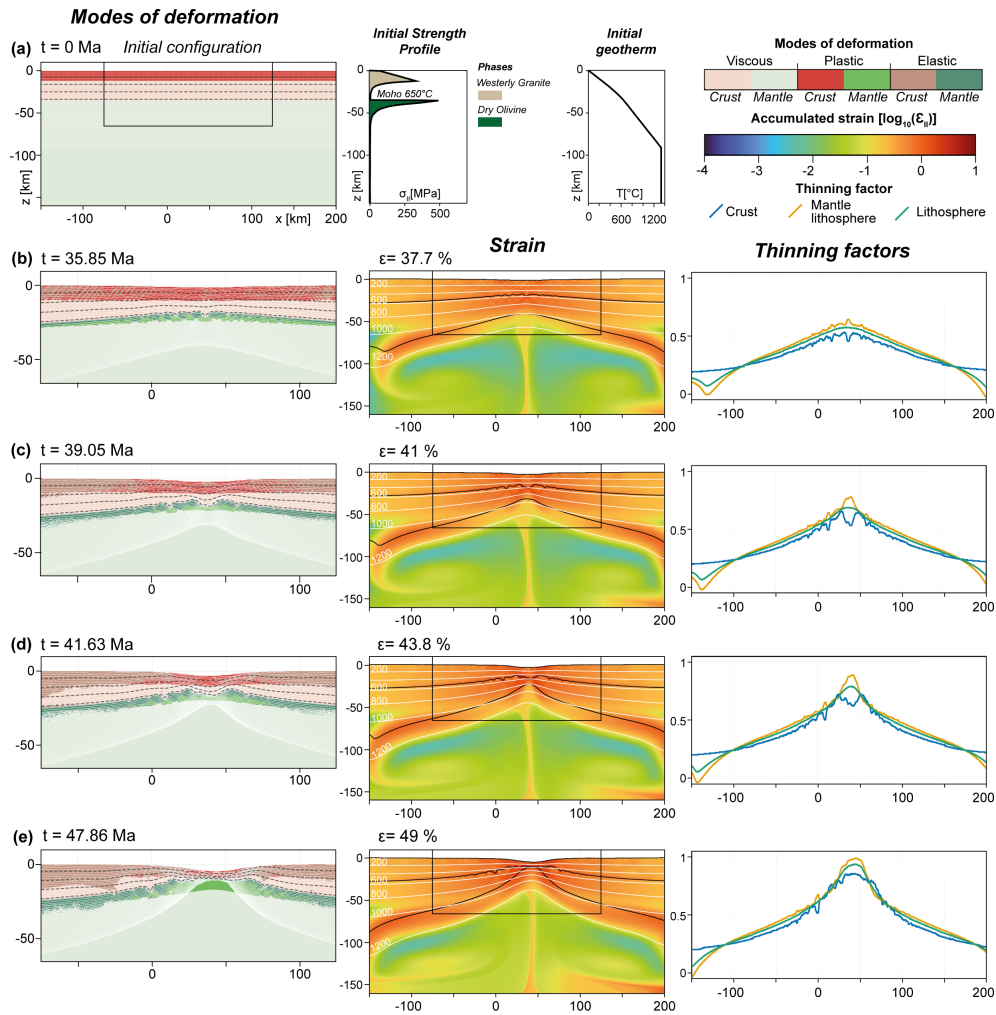
Figure 5. Numerical model NR07 illustrates the development of rifting with initial Moho temperature of 650 °C and a constant bulk extension rate of 0.333×10^{-15} s^{-1}. Left column represents an enlargement of the model showing the mode of deformations and their evolution during ongoing extension. The doted gray and thin white lines represent passive markers. Please note that the middle one represents the initial plastic-elastic to viscous transition (i.e., brittle–ductile transition). The central column documents the accumulated von Mises strain (εII). The white contours show the isotherms in °C. The right column displays the thinning factor distribution across the model for the crust, the mantle lithosphere and the whole lithosphere.

5. Necking and thinning continental lithosphere: synthesis and discussion

5.1. *Different modes of lithospheric thinning*

Different modes of lithospheric thinning exist, shaping end-member rifted margin crustal geometries, as illustrated by our simulations (Figures 3–6) and previous models [Brun, 2002, Kusznir and Karner, 2007, Huismans and Beaumont, 2007, 2011, 2014, Brune et al., 2014, 2017, Svartman Dias et al., 2015, Pérez-Gussinyé et al., 2023]. Here, we show the distribution between elastic, plastic and viscous deformation in the crust and mantle for each stage of our
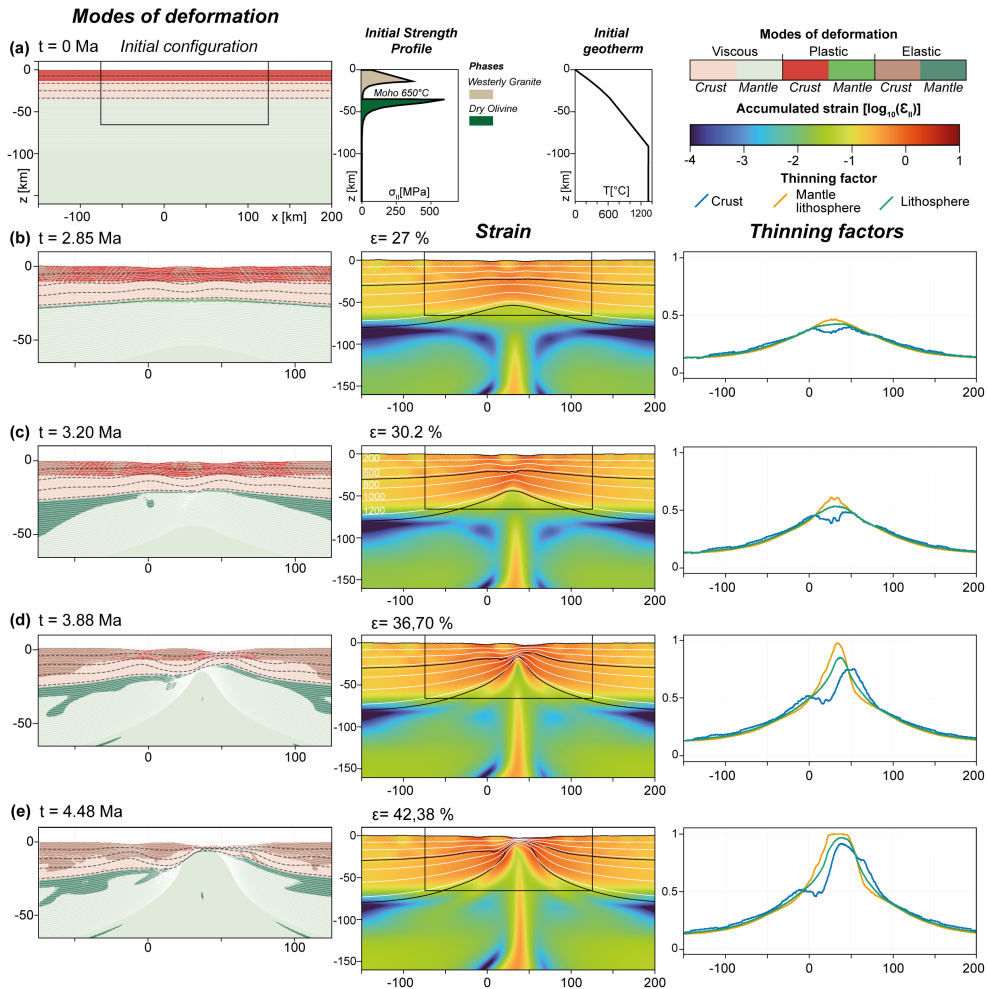
Figure 6. Numerical model NR09 illustrates the development of rifting with initial Moho temperature of 650 °C and a constant bulk extension rate of 3×10^{-15} s^{-1}. Left column represents an enlargement of the model showing the mode of deformations and their evolution during ongoing extension. The doted gray and thin white lines represent passive markers. Please note that the middle one represents the initial plastic-elastic to viscous transition (i.e., brittle–ductile transition). The central column documents the accumulated von Mises strain (εII). The white contours show the isotherms in °C. The right column displays the thinning factor distribution across the model for the crust, the mantle lithosphere and the whole lithosphere.

models. The flowing or non-flowing behaviour of the lower crust is controlled by its strength, which determines its efficiency as a decoupling layer. The strength of the viscous lower crust depends on both temperature and extension rates [Brun, 2002], evolving during extension: viscous material strengthens for higher strain rates and weakens with increasing temperature [Brun, 2002, see also review by Pérez-

Gussinyé and Liu, 2022]. More generally, extensional modes and final rifted margin morphology are controlled by the presence or absence of decoupling levels within the lithosphere [Buck, 1991, Huet et al., 2011a, Brun and Beslier, 1996, Duretz et al., 2016].

Our simple two-layer models with only varying initial thermal and boundary conditions, enable us to reproduce the classical narrow and wide modes of

extension defined by Buck [1991]. Our conditions designed to evolve into rifted margins do not reproduce the last core complex mode. This mode would either require higher temperatures at the Moho (>800 °C) and thicker initial crustal thicknesses (>45 km) [Tirel et al., 2008] or a reversed/post-orogenic stratification of the lithosphere leading to the presence of a felsic lower crust [Huet et al., 2011a].

5.1.1. *Thinning cold lithosphere: narrow and localized lithospheric thinning*

Thinning in cold and strong lithosphere results in rapid and narrow strain localization, within conjugate deformation zones in the crust and viscous mantle (NR01, NR03, Figure 7).

Extensional shear zones in forming necking zones accommodate localized crustal thinning and delimit in their hanging wall a comparatively less thinned crustal keystone (Figure 7). Although little brittle deformation is recorded at this stage in the keystone, ductile deformation is recorded in the ductile/viscous lower crust, accommodating the boudinage and necking of the brittle/plastic upper mantle [Figure 2C, Brun and Beslier, 1996]. Enhanced conductive cooling generated by slow extension rates will favour the brittle deformation of the upper mantle and its smaller wavelength boudinage. Depending on the distributed or localized boudinage of the upper mantle layer, the crust of the keystone is more or less heterogeneously thinned (compare NR01 and NR03 in Figure 7), possibly even thickened by lower crustal flow (Figure 2E) according to Chenin et al. [2018]. Depending on extension rates and on crustal thickness heterogeneities in the keystone, final crustal thinning occurs after the keystone is delaminated during strain migration towards the rift axis (NR01) or separated in two symmetric parts enhanced by the coupling between the viscous lower crust and mantle (NR03) (Figure 8).

5.1.2. *Thinning hot lithosphere: wide and distributed thinning*

Thinning in hot and weak lithosphere is associated with delayed strain localization. The weak lower crust is efficient at decoupling between the brittle upper crust and the mantle, generating a wide rift. Ductile deformation is dominant during lithosphere thinning, controlled by the thick viscous lower crust (NR07, NR09, Figure 7).

Slow extension favours active mantle upwelling in the early stage of lithosphere thinning (Figure 2I) [Huismans et al., 2001] associated with a distributed extension and very progressive lithosphere thinning. Slow extension rates will favour conductive cooling and formation of brittle/plastic upper mantle layer thickening toward the rift axis. Boudinage and necking of this layer are associated to a change from wide to narrow extensional mode, recorded by several generations of high-angle normal faults in the brittle upper part of the crust (polyphase faulting, Figure 2F). Strain localization at the rift axis occurs as the continental crust is already significantly thinned (Figure 7). Two conjugate extensional shear zones delimit a narrow central graben that is quickly separated into two symmetric parts (Figure 8).

Fast extension is associated with the boudinage of the brittle/plastic upper crust (Figure 2C), while ductile/viscous deformation is dominant underneath. Strain is accommodated by the simultaneous formation of brittle deformation zones in the upper crust separating weakly deformed crustal blocks, located in a footwall position relative to extensional shear zones. Crustal thinning between these crustal blocks is accommodated by the formation of domes of deeper lower crustal levels, subsequently embrittled (Figure 7). Strain localization in the mantle and in the upper crust is spatially offset. The coupling between the viscous lower crust and mantle at the rift axis below one of these crustal blocks will subsequently generate simple-shear deformation accommodated along a single extensional shear zone.

5.2. *Rifted margin morphologies and comparison with modelling results*

Rifted margins show a large variability in width, either related to a localized crustal thinning or showing smoother crustal thinning over very large distances. Conjugate profiles either show symmetric or asymmetric crustal structures (Figure 1). This diversity depends on the modes of lithospheric thinning (Figures 7 and 8) as shown by numerical and analogue models [Brun, 2002, Kusznir and Karner, 2007, Huismans and Beaumont, 2011, 2014, Brune et al., 2014, 2017, Pérez-Gussinyé et al., 2023]. Little asymmetry is observed because the initial and boundary conditions are mostly symmetric [Duretz et al., 2021]. Previous numerical studies showed that the final
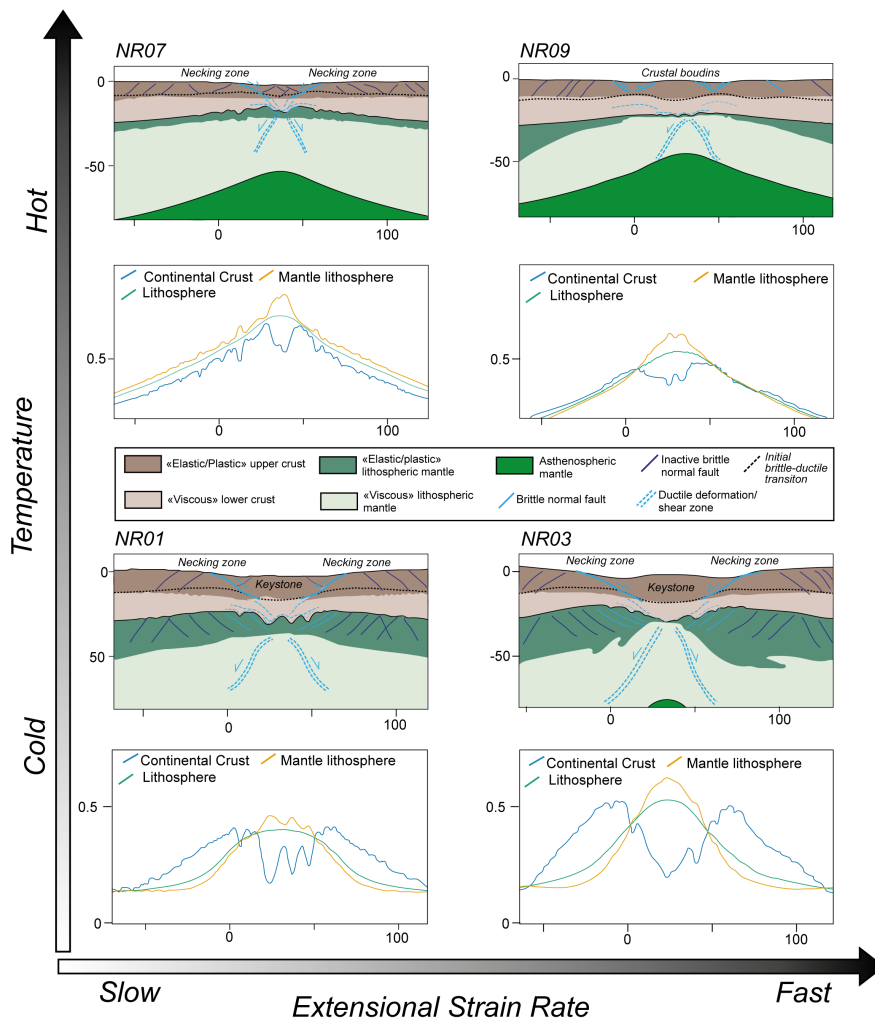
Figure 7. Synthetic diagrams showing the various modes of lithospheric thinning and thinning factors during the early development of necking zones depending on the initial Moho temperature and extensional rates.

morphology of rifted margins and the degree of symmetry or asymmetry largely depend on the feedback between lithosphere strength, extension rates and applied initial and boundary conditions [Tetreault and Buiter, 2018, Svartman Dias et al., 2015, Duretz et al., 2016]. In addition, the degree of symmetry or asymmetry is also related to the efficiency of strain and strain-rate softening processes [Gueydan et al., 2008, Huismans and Beaumont, 2003] as well as structural inheritance [Le Pourhiet et al., 2004, Huet et al., 2011a,b, Petri et al., 2019, Balázs et al., 2018] which were not explored in our study.

Although it is challenging to compare numerical modelling results with natural examples directly, numerical simulations can be used to understand some stages of the evolution of rifted margins.

5.2.1. *Narrow rifted margins*

Narrow lithospheric thinning is commonly observed in relatively magma-poor Atlantic-type rifted margins (Figure 1a/l) and in some segments of the South Atlantic margin [e.g., Péron-Pinvidic et al., 2017]. Rifted margins typically show a localized zone of intense crustal thinning ranging between 50 km
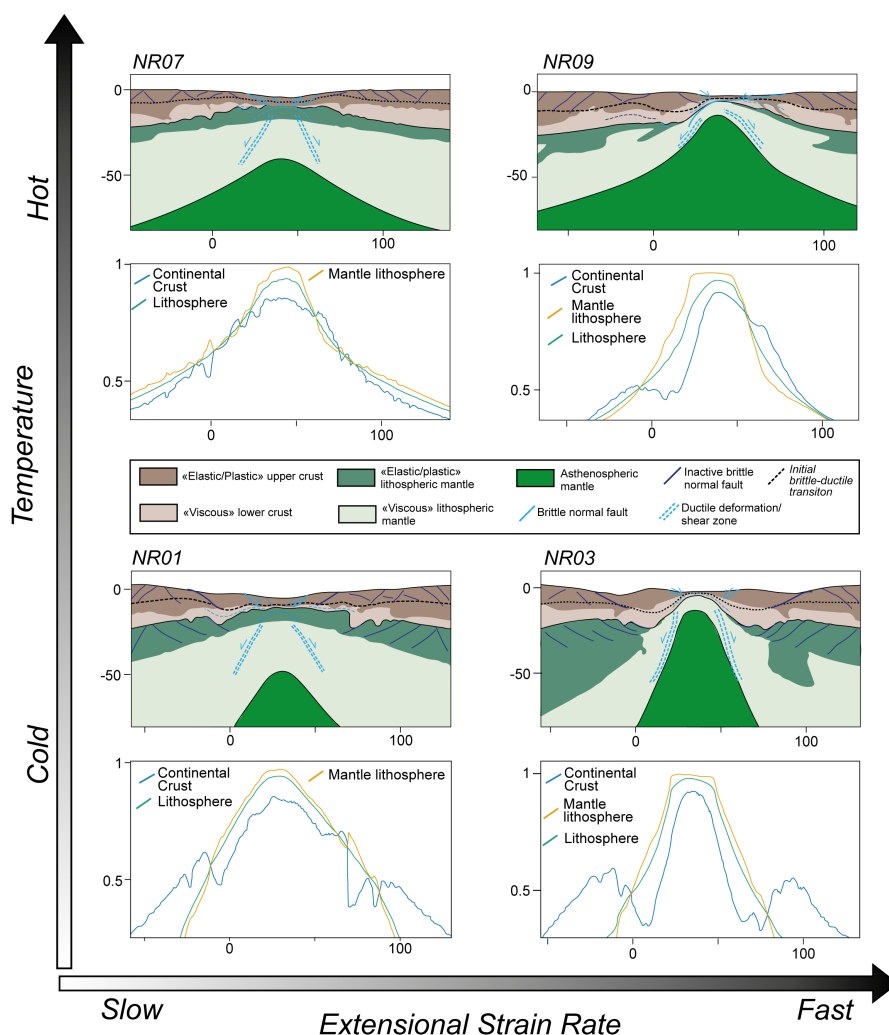
Figure 8. Synthetic diagrams showing the different of modes of lithospheric thinning and thinning factors during the late development of necking zones and distal margins depending on the initial Moho temperature and extensional rates.

to 100 km distance (i.e., the necking zone). Crustal thinning in the necking zones is accommodated by large offset extensional shear zones (i.e., detachment faults) that exhume deeper crustal levels (Figures 7 and 8). As deeper crustal levels are exhumed, they are, however, progressively embrittled (note in Figures 7 and 8 the exhumation in the brittle field of the passive marker indicative of the initial brittle–ductile transition). Detachment faults associated with the formation of necking zones have notably been identified in remnants of the Alpine Tethys margins [Mohn et al., 2012, Ribes et al., 2020, Dall'Asta et al., 2022]

and in the Pyrenees [Masini et al., 2014, Tugend et al., 2015].

In the initial stage of lithospheric thinning (Figure 7), these detachments delimit a relatively weakly thinned crustal keystone. This crustal block is subsequently either delaminated or cut in two parts, determining the symmetry or asymmetry of conjugate distal rifted margins (Figure 8). Delamination of this keystone is associated to the migration of extensional faulting [as expected for sequential faulting: Ranero and Pérez-Gussinyé, 2010] and progressive crustal embrittlement [Pérez-Gussinyé and Reston,

2001] (NR01, Figure 8). Conjugate pairs of rifted margins will show a partly preserved crustal block on one side, while the other one shows intense faulting. This block can also be separated in roughly symmetric parts (NR03, Figure 8) associated with limited or no crustal embrittlement, in which case both conjugate rifted margins will show a crustal block preserved in their distal margin. The timing of extensional faulting (Figures 7 and 8) and the isostatic evolution [Chenin et al., 2018] of this keystone differ from that recorded in adjacent necking zones with only the earliest and latest faulting stages being recorded. Since this keystone is not necessarily preserved as such in present-day rifted margins, its recognition remains interpretative. Delaminated remnants of this keystone have been interpreted in present-day rifted margins [e.g., Iberia–Newfoundland: Péron-Pinvidic and Manatschal, 2010; Angola–Gabon: Péron-Pinvidic et al., 2017]. Because of its atypical sedimentary record [Lemoine et al., 1987, Mohn et al., 2010], the Briançonnais domain of the Alpine Tethys is often considered as a fossil analogue of this keystone block [Mohn et al., 2012].

In summary, the evolution of NR01 is relatively consistent with that of sedimentary starved magma-poor rifted margins such as Iberia–Newfoundland [Sutra et al., 2013, Mohn et al., 2015] or from the fossil Alpine Tethys [Manatschal, 2004, Mohn et al., 2010]. The general evolution of NR03 is however less realistic because of the high extension rates from the onset of rifting. Results of the simulations cannot straightforwardly be compared to natural examples. Such high velocities from the onset of rifting could potentially occur in 3D in the case of rifting at the tip of an oceanic propagator [Le Pourhiet et al., 2018, Jourdon et al., 2020].

5.2.2. *Wide rifted margins*

Wide zones of lithospheric thinning are observed in some marginal seas (e.g., South China Sea: Figure 1m–o; Alarcon segment of the Gulf of California: Figure 1q) that are expected to form in higher geothermal gradients. Such rifted margins typically show a wide zone (>200 km) of progressive crustal thinning (diffuse necking zones). Examples such as the South China Sea rifted margins typically show a succession of rift basins under which the crust is thinned to extremely thinned that are separated by thicker crustal blocks (Figure 1m/o) [Pichot et al.,

2014, Clerc et al., 2018, Nirrengarten et al., 2020]. Such a situation is comparable to model NR09 characterized by the formation of upper crustal boudins (Figures 7 and 8). Between these boudins, domes of lower crust are observed below rift basins and are embrittled with increasing exhumation (see evolution of the passive marker indicating the initial brittle–ductile transition in Figures 7 and 8). Exhumation of deep crustal levels along low-angle extensional faults is documented in several rift basins of the South China Sea [Liwan basin: Deng et al., 2020; Dangerous Ground: Liang et al., 2019]. Reflective patterns in some of these domes are interpreted as folds attesting the initial ductile behaviour of the exhumed crust [Deng et al., 2020]. Synchronous basins are formed during upper crustal boudinage (NR09, Figure 7), as suggested for the South China Sea based on stratigraphic correlations [Cameselle et al., 2020].

In summary, the evolution of NR07 and NR09 shows typical features of a wide rift [Buck, 1991]. Rifted margins formed subsequently to wide rifting modes are observed in some marginal basins of Southeast Asia. Marginal seas are however generally characterized by high extension rates as observed in NR09 [Woodlark Basin: Abers, 2001; South China Sea: Larsen et al., 2018, Mohn et al., 2022]. Such high velocities likely result from boundary conditions, controlled by adjacent subduction zones [Mohn et al., 2022, Larvet et al., 2023].

5.2.3. *Limitations*

It should be noted that magmatism or serpentinization processes are not included in the models. Serpentinization is expected to occur in magma-poor systems during the latest stage of crustal thinning controlling the structural style during mantle exhumation [Gillard et al., 2019]. In normal conditions, magma is expected to be generated for thinning factors of 0.7 or even 0.5, for higher geothermal gradients. Magmatic rocks would likely be emplaced prior to or during the latest stage of lithospheric thinning associated with the formation of a sharp COT adjacent to the oceanic crust as observed in the South China Sea [Larsen et al., 2018, Nirrengarten et al., 2020]. Onset of magmatism during earlier stages of crustal thinning could even be associated with the formation of seaward-dipping reflectors.

5.3. *Evolution of depth-dependent thinning and comparison with rifted margins*

Depth-dependent thinning has previously been recognized in present-day rifted margins, showing that extensional faulting identified in the upper crust could not balance the amount of thinning measured at the scale of the whole crust or lithosphere [Davis and Kusznir, 2004, Reston, 2007b]. Based on the increasingly higher resolution of seismic data, several studies show that most of this *crustal* DDT [Svartman Dias et al., 2016] could be attributed to sub-seismic extensional faulting, non-recognition of polyphase faulting [Reston, 2007a,b] or of top-basement detachment faults [Gomez-Romeu et al., 2020].

Thinning factors extracted from our models enables us to compare the evolution through time of the whole crust, mantle and whole lithosphere thinning. Except for whole crustal thinning factors, these measurements are not easily obtained in natural systems. Lithosphere thinning in natural systems is generally approximated from subsidence analysis in rift basins and do not greatly differ from whole crust thinning factors where they can be measured [Davis and Kusznir, 2004]. Thinning factors extracted from our models show an important discrepancy between crustal thinning and mantle or lithosphere thinning (Figures 7 and 8) [Huismans and Beaumont, 2011; *lithospheric* DDT in Svartman Dias et al., 2016] that cannot be measured in present-day margins.

Lithospheric DDT in narrow rift models is particularly contrasted in time and space. The early stage of lithospheric thinning is associated to initially greater crustal than mantle thinning in rift shoulders where necking zones are progressively formed, while at the rift axis (location of the keystone), mantle thinning exceeds crustal thinning (Figure 7). Part of this DDT is, however, transient and is partly erased by subsequent crustal thinning (Figure 8). Hence at the end of rifting, little depth-dependent thinning is observed between the crust and mantle/lithosphere in the distal margins. Lithospheric DDT is also seen in our wide rift models but is either less pronounced after lithospheric thinning (NR07) or reflects asymmetric thinning (NR09).

Although difficult to measure in natural systems, lithospheric scale DDT is predicted by numerical simulations, part is permanently recorded (rift shoulders, where necking zones form), part is transient (at the rift axis). Hence, thinning factors measured in present-day margins are only partly representative of the magnitude and distribution of DDT, although its consequences for the subsidence evolution will be recorded in the stratigraphic record.

6. Conclusions and perspectives

We reviewed the mechanisms of continental lithospheric thinning and the associated extensional structures that control the formation of rifted margins and their observed diverse crustal geometries. Using a simple two-layer model for the crust and mantle, we illustrate the spatial and temporal evolution of extensional modes for different initial thermal conditions and extension rates. Different modes of lithospheric thinning are highlighted that control the formation of end-member rifted margin morphologies observed in natural systems. We show as previously known that lithosphere thinning is indeed depth-dependent [Davis and Kusznir, 2004, Huismans and Beaumont, 2011, 2014], notably during the formation of rift shoulders and necking zones. Transient phases of lithospheric DDT are also observed in modelling results that cannot easily be measured in natural systems.

Here, only the results of 2D numerical simulations are presented and compared to natural systems. More and more 3D numerical models are being developed, testing the effect of obliquity or lateral changes in boundary conditions [Brune and Autin, 2013, Ammann et al., 2018, Duclaux et al., 2020, Jourdon et al., 2021], changes of extensional modes due to propagation [Le Pourhiet et al., 2018, Jourdon et al., 2020] or changes in polarity and asymmetry due to inheritance [Le Pourhiet et al., 2017, Balázs et al., 2018, Neuharth et al., 2021]. The development of 3D models and their comparison with natural systems will certainly continue to enhance our understanding of rifting processes in the near future.

Declaration of interests

The authors do not work for, advise, own shares in, or receive funds from any organization that could benefit from this article, and have declared no affiliations other than their research organizations.

Acknowledgments

We thank François Sapin and another anonymous reviewer for their thoughtful suggestions and Olivier Fabbri for a careful final revision of the text. Our gratitude also goes to N. J. Kusznir for our extensive and enlightening discussions on lithosphere thinning mechanisms.

Supplementary data

Supporting information for this article is available on the journal's website under https://doi.org/10.5802/crgeos.257 or from the author.

References

Abers, G. A. (2001). Evidence for seismogenic normal faults at shallow dips in continental rifts. *Geol. Soc. Lond. Spec. Publ.*, 187(1), 305–318.

Afilhado, A., Moulin, M., Aslanian, D., Schnuerle, P., Klingelhoefer, F., Nouze, H., et al. (2015). Deep crustal structure across a young passive margin from wide-angle and reflection seismic data (The SARDINIA Experiment)–II. Sardinia's margin. *Bull. Soc. Géol. Fr.*, 186(4–5), 331–351.

Afiri, A., Gueydan, F., Pitra, P., Essaifi, A., and Précigout, J. (2011). Oligo-Miocene exhumation of the Beni-Bousera peridotite through a lithosphere-scale extensional shear zone. *Geodin. Acta*, 24(1), 49–60.

Ammann, N., Liao, J., Gerya, T., and Ball, P. (2018). Oblique continental rifting and long transform fault formation based on 3D thermomechanical numerical modeling. *Tectonophysics*, 746, 106–120.

Anderson, E. M. (1951). *The Dynamics of Faulting*. Oliver and Boyd, Edinburgh, 2nd edition.

Artyushkov, E. V. (1973). Stresses in the lithosphere caused by crustal thickness inhomogeneities. *J. Geophys. Res.*, 78(32), 7675–7708.

Aumar, C., Merle, O., Bosse, V., and Monié, P. (2022). Syn-rift Cretaceous deformation in the Agly Variscan Massif (Eastern Pyrenees, France). *BSGF-Earth Sci. Bull.*, 193(1), article no. 6.

Balázs, A., Matenco, L., Vogt, K., Cloetingh, S., and Gerya, T. (2018). Extensional polarity change in continental rifts: Inferences from 3-D numerical modeling and observations. *J. Geophys. Res.: Solid Earth*, 123(9), 8073–8094.

Batchelor, G. (1967). *An Introduction to Fluid Dynamics*. Cambridge University Press, New York.

Beaumont, C. and Ings, S. J. (2012). Effect of depleted continental lithosphere counterflow and inherited crustal weakness on rifting of the continental lithosphere: General results. *J. Geophys. Res.: Solid Earth*, 117(B8), article no. B08407.

Bellahsen, N., Fournier, M., d'Acremont, E., Leroy, S., and Daniel, J. M. (2006). Fault reactivation and rift localization: Northeastern Gulf of Aden margin. *Tectonics*, 25(1), article no. TC1007.

Bessière, E., Jolivet, L., Augier, R., Scaillet, S., Précigout, J., Azanón, J. M., et al. (2021). Lateral variations of pressure-temperature evolution in non-cylindrical orogens and 3-D subduction dynamics: the Betic-Rif Cordillera example. *Bull. Soc. Géol. Fr. - Earth Sci. Bull.*, 192(1), article no. 8.

Biari, Y., Klingelhoefer, F., Sahabi, M., Aslanian, D., Schnurle, P., Berglar, K., et al. (2015). Deep crustal structure of the North-West African margin from combined wide-angle and reflection seismic data (MIRROR seismic survey). *Tectonophysics*, 656, 154–174.

Bissig, T. and Hermann, J. (1999). From pre-Alpine extension to Alpine convergence: the example of the southwestern margin of the Margna nappe (Val Malenco, N-Italy). *Schweiz. Miner. Petrogr. Mitt.*, 79(3), 363–380.

Block, L. and Royden, L. H. (1990). Core complex geometries and regional scale flow in the lower crust. *Tectonics*, 9(4), 557–567.

Boillot, G., Grimaud, S., Mauffret, A., Mougenot, D., Kornprobst, J., Mergoil-Daniel, J., and Torrent, G. (1980). Ocean-continent boundary off the Iberian margin: a serpentinite diapir west of the Galicia Bank. *Earth Planet. Sci. Lett.*, 48(1), 23–34.

Boillot, G., Recq, M., Winterer, E. L., Meyer, A. W., Applegate, J., Baltuck, M., et al. (1987). Tectonic denudation of the upper mantle along passive margins: a model based on drilling results (ODP leg 103, western Galicia margin, Spain). *Tectonophysics*, 132(4), 335–342.

Brady, R., Wernicke, B., and Fryxell, J. (2000). Kinematic evolution of a large-offset continental normal fault system, South Virgin Mountains, Nevada. *Geol. Soc. Am. Bull.*, 112(9), 1375–1397.

Braun, J. and Beaumont, C. (1987). Styles of continental rifting: results from dynamic models of lithospheric extension. In Beaumont, C. and

Tankard, A. J., editors, *Sedimentary Basins and Basin-Forming Mechanisms*, volume 12 of *Canadian Society of Petroleum Geologists Memoir*, pages 241–258.

Braun, M. G., Hirth, G., and Parmentier, E. M. (2000). The effects of deep damp melting on mantle flow and melt generation beneath mid-ocean ridges. *Earth Planet. Sci. Lett.*, 176(3–4), 339–356.

Brun, J. P. (1999). Narrow rifts versus wide rifts: inferences for the mechanics of rifting from laboratory experiments. *Philos. Trans. R. Soc. Lond. A*, 357(1753), 695–712.

Brun, J. P. (2002). Deformation of the continental lithosphere: Insights from brittle-ductile models. *Geol. Soc. Lond. Spec. Publ.*, 200(1), 355–370.

Brun, J. P. and Beslier, M. O. (1996). Mantle exhumation at passive margins. *Earth Planet. Sci. Lett.*, 142(1–2), 161–173.

Brun, J. P., Sokoutis, D., and Van Den Driessche, J. (1994). Analogue modeling of detachment fault systems and core complexes. *Geology*, 22(4), 319–322.

Brune, S. and Autin, J. (2013). The rift to break-up evolution of the Gulf of Aden: Insights from 3D numerical lithospheric-scale modelling. *Tectonophysics*, 607, 65–79.

Brune, S., Heine, C., Clift, P. D., and Pérez-Gussinyé, M. (2017). Rifted margin architecture and crustal rheology: reviewing Iberia-Newfoundland, central South Atlantic, and South China Sea. *Mar. Petrol. Geol.*, 79, 257–281.

Brune, S., Heine, C., Pérez-Gussinyé, M., and Sobolev, S. V. (2014). Rift migration explains continental margin asymmetry and crustal hyper-extension. *Nat. Commun.*, 5(1), article no. 4014.

Buck, W. R. (1988). Flexural rotation of normal faults. *Tectonics*, 7(5), 959–973.

Buck, W. R. (1991). Modes of continental lithospheric extension. *J. Geophys. Res.: Solid Earth*, 96(B12), 20161–20178.

Buck, W. R., Lavier, L. L., and Poliakov, A. N. (1999). How to make a rift wide. *Philos. Trans. R. Soc. Lond. A*, 357(1753), 671–693.

Burov, E. and Poliakov, A. (2001). Erosion and rheology controls on synrift and postrift evolution: Verifying old and new ideas using a fully coupled numerical model. *J. Geophys. Res.: Solid Earth*, 106(B8), 16461–16481.

Cameselle, A. L., Ranero, C. R., and Barckhausen,

U. (2020). Understanding the 3D formation of a wide rift: The central South China Sea rift system. *Tectonics*, 39(12), article no. e2019TC006040.

Chenin, P., Manatschal, G., Picazo, S., Müntener, O., Karner, G., Johnson, C., and Ulrich, M. (2017). Influence of the architecture of magma-poor hyperextended rifted margins on orogens produced by the closure of narrow versus wide oceans. *Geosphere*, 13(2), 559–576.

Chenin, P., Schmalholz, S. M., Manatschal, G., and Karner, G. D. (2018). Necking of the lithosphere: A reappraisal of basic concepts with thermomechanical numerical modeling. *J. Geophys. Res.: Solid Earth*, 123(6), 5279–5299.

Clerc, C., Jolivet, L., and Ringenbach, J. C. (2015). Ductile extensional shear zones in the lower crust of a passive margin. *Earth Planet. Sci. Lett.*, 431, 1–7.

Clerc, C. and Lagabrielle, Y. (2014). Thermal control on the modes of crustal thinning leading to mantle exhumation: Insights from the Cretaceous Pyrenean hot paleomargins. *Tectonics*, 33(7), 1340–1359.

Clerc, C., Ringenbach, J. C., Jolivet, L., and Ballard, J. F. (2018). Rifted margins: Ductile deformation, boudinage, continentward-dipping normal faults and the role of the weak lower crust. *Gondwana Res.*, 53, 20–40.

Cloetingh, S., Burov, E., Matenco, L., Beekman, F., Roure, F., and Ziegler, P. A. (2013). The Moho in extensional tectonic settings: Insights from thermomechanical models. *Tectonophysics*, 609, 558–604.

Collettini, C. (2011). The mechanical paradox of low-angle normal faults: Current understanding and open questions. *Tectonophysics*, 510(3–4), 253–268.

Dall'Asta, N., Hoareau, G., Manatschal, G., Centrella, S., Denèle, Y., Ribes, C., and Kalifi, A. (2022). Structural and petrological characteristics of a Jurassic detachment fault from the Mont-Blanc massif (Col du Bonhomme area, France). *J. Struct. Geol.*, 159, article no. 104593.

Davis, J. K. and Lavier, L. L. (2017). Influences on the development of volcanic and magma-poor morphologies during passive continental rifting. *Geosphere*, 13(5), 1524–1540.

Davis, M. and Kusznir, N. (2004). Depth-dependent lithospheric stretching at rifted continental margins. In *Rheology and Deformation of the Lithosphere at Continental Margins*, pages 92–137.

Columbia University Press, New York.

de Borst, R. and Duretz, T. (2020). On viscoplastic regularisation of strain-softening rocks and soils. *Int. J. Numer. Anal. Methods Geomech.*, 44(6), 890–903.

Dean, S. M., Minshull, T. A., Whitmarsh, R. B., and Louden, K. E. (2000). Deep structure of the ocean-continent transition in the southern Iberia Abyssal Plain from seismic refraction profiles: The IAM-9 transect at 40 20′ N. *J. Geophys. Res.: Solid Earth*, 105(B3), 5859–5885.

Deng, H., Ren, J., Pang, X., Rey, P. F., McClay, K. R., Watkinson, I. M., et al. (2020). South China Sea documents the transition from wide continental rift to continental break up. *Nat. Commun.*, 11(1), article no. 4583.

Desmurs, L., Manatschal, G., and Bernoulli, D. (2001). The Steinmann Trinity revisited: mantle exhumation and magmatism along an ocean-continent transition: the Platta nappe, eastern Switzerland. *Geol. Soc. Lond. Spec. Publ.*, 187(1), 235–266.

Dewey, J. F. and Bird, J. M. (1970). Mountain belts and the new global tectonics. *J. Geophys. Res.*, 75(14), 2625–2647.

Driscoll, N. W. and Karner, G. D. (1998). Lower crustal extension across the Northern Carnarvon basin, Australia: Evidence for an eastward dipping detachment. *J. Geophys. Res.: Solid Earth*, 103(B3), 4975–4991.

Duclaux, G., Huismans, R. S., and May, D. A. (2020). Rotation, narrowing, and preferential reactivation of brittle structures during oblique rifting. *Earth Planet. Sci. Lett.*, 531, article no. 115952.

Duretz, T., de Borst, R., and Le Pourhiet, L. (2019). Finite thickness of shear bands in frictional viscoplasticity and implications for lithosphere dynamics. *Geochem. Geophys. Geosyst.*, 20(11), 5598–5616.

Duretz, T., de Borst, R., and Yamato, P. (2021). Modeling lithospheric deformation using a compressible visco-elasto-viscoplastic rheology and the effective viscosity approach. *Geochem. Geophys. Geosyst.*, 22(8), article no. e2021GC009675.

Duretz, T., de Borst, R., Yamato, P., and Le Pourhiet, L. (2020). Towards robust and predictive geodynamic modelling: the way forward in frictional plasticity. *Geophys. Res. Lett.*, 47(5), article no. e2019GL086027.

Duretz, T., Petri, B., Mohn, G., Schmalholz, S. M., Schenker, F. L., and Müntener, O. (2016). The importance of structural softening for the evolution and architecture of passive margins. *Sci. Rep.*, 6(1), article no. 38704.

Eldholm, O., Skogseid, J., Planke, S., and Gladczenko, T. P. (1995). Volcanic margin concepts. In Banda, E., Torné, M., and Talwani, M., editors, *Rifted Ocean-Continent Boundaries*, volume 463 of *NATO ASI Series*. Springer, Dordrecht.

Falvey, D. A. (1974). The development of continental margins in plate tectonic theory. *APPEA J.*, 14(1), 95–106.

Fazlikhani, H., Fossen, H., Gawthorpe, R. L., Faleide, J. I., and Bell, R. E. (2017). Basement structure and its influence on the structural configuration of the northern North Sea rift. *Tectonics*, 36(6), 1151–1177.

Fletcher, R., Kusznir, N., and Cheadle, M. (2009). Melt initiation and mantle exhumation at the Iberian rifted margin: Comparison of pure–shear and upwelling-divergent flow models of continental breakup. *C. R. Géosci.*, 341(5), 394–405.

Fossen, H. (2010). Extensional tectonics in the North Atlantic Caledonides: a regional view. *Geol. Soc. Lond. Spec. Publ.*, 335(1), 767–793.

Frasca, G., Gueydan, F., Brun, J. P., and Monié, P. (2016). Deformation mechanisms in a continental rift up to mantle exhumation. Field evidence from the western Betics, Spain. *Mar. Petrol. Geol.*, 76, 310–328.

Frizon de Lamotte, D., Fourdan, B., Leleu, S., Lepar-mentier, F., and de Clarens, P. (2015). Style of rifting and the stages of Pangea breakup. *Tectonics*, 34(5), 1009–1029.

Froitzheim, N. and Eberli, G. P. (1990). Extensional detachment faulting in the evolution of a Tethys passive continental margin, Eastern Alps, Switzerland. *Geol. Soc. Am. Bull.*, 102(9), 1297–1308.

Funck, T., Erlendsson, Ö., Geissler, W. H., Gradmann, S., Kimbell, G. S., McDermott, K., and Petersen, U. K. (2017). A review of the NE Atlantic conjugate margins based on seismic refraction data. *Geol. Soc. Lond. Spec. Publ.*, 447(1), 171–205.

Funck, T., Hopper, J. R., Larsen, H. C., Louden, K. E., Tucholke, B. E., and Holbrook, W. S. (2003). Crustal structure of the ocean-continent transition at Flemish Cap: Seismic refraction results. *J. Geophys. Res.: Solid Earth*, 108(B11), article

no. 2531.

Funck, T., Jackson, H. R., Louden, K. E., Dehler, S. A., and Wu, Y. (2004). Crustal structure of the northern Nova Scotia rifted continental margin (eastern Canada). *J. Geophys. Res.: Solid Earth*, 109(B9), article no. B09102.

Gautier, P., Brun, J. P., and Jolivet, L. (1993). Structure and kinematics of upper Cenozoic extensional detachment on Naxos and Paros (Cyclades Islands, Greece). *Tectonics*, 12(5), 1180–1194.

Geoffroy, L., Burov, E., and Werner, P. (2015). Volcanic passive margins: another way to break up continents. *Sci. Rep.*, 5, article no. 14828.

Gerya, T. V. and Yuen, D. A. (2003). Characteristics-based marker-in-cell method with conservative finite-differences schemes for modeling geological flows with strongly variable transport properties. *Phys. Earth Planet. Inter.*, 140(4), 293–318.

Gillard, M., Tugend, J., Müntener, O., Manatschal, G., Karner, G. D., Autin, J., et al. (2019). The role of serpentinization and magmatism in the formation of decoupling interfaces at magma-poor rifted margins. *Earth-Sci. Rev.*, 196, article no. 102882.

Goetze, C. and Evans, B. (1979). Stress and temperature in the bending lithosphere as constrained by experimental rock mechanics. *Geophys. J. Int.*, 59(3), 463–478.

Gomez-Romeu, J., Kusznir, N., Roberts, A., and Manatschal, G. (2020). Measurements of the extension required for crustal breakup on the magma-poor Iberia-Newfoundland conjugate margins. *Mar. Petrol. Geol.*, 118, article no. 104403.

Gresseth, J. L. S., Osmundsen, P. T., and Péron-Pinvidic, G. (2023). 3D evolution of detachment fault systems in necking domains: Insights from the Klakk Fault Complex and the Frøya High, mid-Norwegian rifted margin. *Tectonics*, 42(3), article no. e2022TC007600.

Gueydan, F., Leroy, Y. M., and Jolivet, L. (2001). Grain-size-sensitive flow and shear-stress enhancement at the brittle–ductile transition of the continental crust. *Int. J. Earth Sci.*, 90(1), 181–196.

Gueydan, F., Morency, C., and Brun, J. P. (2008). Continental rifting as a function of lithosphere mantle strength. *Tectonophysics*, 460(1–4), 83–93.

Gueydan, F., Pitra, P., Afiri, A., Poujol, M., Essaifi, A., and Paquette, J. L. (2015). Oligo-Miocene thinning of the Beni Bousera peridotites and their Variscan crustal host rocks, Internal Rif, Morocco. *Tectonics*,

34(6), 1244–1268.

Handy, M. R. and Zingg, A. (1991). The tectonic and rheological evolution of an attenuated cross section of the continental crust: Ivrea crustal section, southern Alps, northwestern Italy and southern Switzerland. *Geol. Soc. Am. Bull.*, 103(2), 236–253.

Hansen, F. D. and Carter, N. L. (1983). Semibrittle creep of dry and wet Westerly Granite at 1000 MPa. In *The 24th U.S. Symposium on Rock Mechanics (USRMS), College Station, Texas, June 20*. ARMA-83-0429.

Heezen, B. C. (1960). The rift in the ocean floor. *Sci. Am.*, 203(4), 98–114.

Hirth, G. and Kohlstedt, D. (2004). Rheology of the upper mantle and the mantle wedge: A view from the experimentalists. In *Inside the Subduction Factory*, pages 83–105. American Geophysical Union (AGU), Washington, DC.

Hölker, A. B., Manatschal, G., Holliger, K., and Bernoulli, D. (2003). Tectonic nature and seismic response of top-basement detachment faults in magma-poor rifted margins. *Tectonics*, 22(4), article no. 1035.

Hopper, J. R. and Buck, W. R. (1996). The effect of lower crustal flow on continental extension and passive margin formation. *J. Geophys. Res.: Solid Earth*, 101(B9), 20175–20194.

Huet, B., Le Pourhiet, L., Labrousse, L., Burov, E., and Jolivet, L. (2011a). Post-orogenic extension and metamorphic core complexes in a heterogeneous crust: the role of crustal layering inherited from collision. Application to the Cyclades (Aegean domain). *Geophys. J. Int.*, 184(2), 611–625.

Huet, B., Le Pourhiet, L., Labrousse, L., Burov, E. B., and Jolivet, L. (2011b). Formation of metamorphic core complex in inherited wedges: A thermomechanical modelling study. *Earth Planet. Sci. Lett.*, 309(3–4), 249–257.

Huismans, R. and Beaumont, C. (2011). Depth-dependent extension, two-stage breakup and cratonic underplating at rifted margins. *Nature*, 473(7345), 74–78.

Huismans, R. S. and Beaumont, C. (2003). Symmetric and asymmetric lithospheric extension: Relative effects of frictional-plastic and viscous strain softening. *J. Geophys. Res.: Solid Earth*, 108(B10), article no. 2496.

Huismans, R. S. and Beaumont, C. (2007). Roles of

lithospheric strain softening and heterogeneity in determining the geometry of rifts and continental margins. *Geol. Soc. Lond. Spec. Publ.*, 282(1), 111–138.

Huismans, R. S. and Beaumont, C. (2014). Rifted continental margins: The case for depth-dependent extension. *Earth Planet. Sci. Lett.*, 407, 148–162.

Huismans, R. S., Buiter, S. J., and Beaumont, C. (2005). Effect of plastic-viscous layering and strain softening on mode selection during lithospheric extension. *J. Geophys. Res.: Solid Earth*, 110(B2), article no. B02406.

Huismans, R. S., Podladchikov, Y. Y., and Cloetingh, S. (2001). Transition from passive to active rifting: Relative importance of asthenospheric doming and passive extension of the lithosphere. *J. Geophys. Res.: Solid Earth*, 106(B6), 11271–11291.

Jammes, S. and Lavier, L. L. (2016). The effect of bimineralic composition on extensional processes at lithospheric scale. *Geochem. Geophys. Geosyst.*, 17(8), 3375–3392.

Jammes, S., Manatschal, G., Lavier, L., and Masini, E. (2009). Tectonosedimentary evolution related to extreme crustal thinning ahead of a propagating ocean: Example of the western Pyrenees. *Tectonics*, 28(4), article no. TC4012.

Jamtveit, B., Austrheim, H., and Putnis, A. (2016). Disequilibrium metamorphism of stressed lithosphere. *Earth-Sci. Rev.*, 154, 1–13.

Jeanniot, L., Kusznir, N., Mohn, G., Manatschal, G., and Cowie, L. (2016). Constraining lithosphere deformation modes during continental breakup for the Iberia–Newfoundland conjugate rifted margins. *Tectonophysics*, 680, 28–49.

Jolivet, L., Gorini, C., Smit, J., and Leroy, S. (2015). Continental breakup and the dynamics of rifting in back-arc basins: The Gulf of Lion margin. *Tectonics*, 34(4), 662–679.

Jolivet, L., Lecomte, E., Huet, B., Denèle, Y., Lacombe, O., Labrousse, L., et al. (2010). The north Cycladic detachment system. *Earth Planet. Sci. Lett.*, 289(1–2), 87–104.

Jourdon, A., Kergaravat, C., Duclaux, G., and Huguen, C. (2021). Looking beyond kinematics: 3D thermo-mechanical modelling reveals the dynamic of transform margins. *Solid Earth Discuss.*, 2021, 1–34.

Jourdon, A., Le Pourhiet, L., Mouthereau, F., and May, D. (2020). Modes of propagation of conti-nental breakup and associated oblique rift structures. *J. Geophys. Res.: Solid Earth*, 125(9), article no. e2020JB019906.

Kaczmarek, M. A. and Müntener, O. (2008). Juxtaposition of melt impregnation and high-temperature shear zones in the upper mantle; field and petrological constraints from the Lanzo Peridotite (Northern Italy). *J. Petrol.*, 49(12), 2187–2220.

Kaczmarek, M. A. and Tommasi, A. (2011). Anatomy of an extensional shear zone in the mantle, Lanzo massif, Italy. *Geochem. Geophys. Geosyst.*, 12(8), article no. Q0AG06.

Kameyama, M., Yuen, D. A., and Karato, S.-I. (1999). Thermal-mechanical effects of low-temperature plasticity (the peierls mechanism) on the deformation of a viscoelastic shear zone. *Earth Planet. Sci. Lett.*, 168(1), 159–172.

Kusznir, N. J. (1991). The distribution of stress with depth in the lithosphere: thermo-rheological and geodynamic constraints. *Philos. Trans. R. Soc. Lond. A*, 337(1645), 95–110.

Kusznir, N. J., Hunsdale, R., Roberts, A. M., and iSIMM Team (2005). Timing and magnitude of depth-dependent lithosphere stretching on the southern Lofoten and northern Vøring continental margins offshore mid-Norway: implications for subsidence and hydrocarbon maturation at volcanic rifted margins. In *Geological Society, London, Petroleum Geology Conference Series*, volume 6, pages 767–783. Geological Society of London.

Kusznir, N. J. and Karner, G. D. (2007). Continental lithospheric thinning and breakup in response to upwelling divergent mantle flow: application to the Woodlark, Newfoundland and Iberia margins. *Geol. Soc. Lond. Spec. Publ.*, 282(1), 389–419.

Kusznir, N. J., Roberts, A. M., and Morley, C. K. (1995). Forward and reverse modelling of rift basin formation. *Geol. Soc. Lond. Spec. Publ.*, 80(1), 33–56.

Lagabrielle, Y., Asti, R., Fourcade, S., Corre, B., Labaume, P., Uzel, J., et al. (2019). Mantle exhumation at magma-poor passive continental margins. Part II: Tectonic and metasomatic evolution of large-displacement detachment faults preserved in a fossil distal margin domain (Saraillé lherzolites, northwestern Pyrenees, France). *Bull. Soc. Géol. Fr.*, 190(1), article no. 14.

Lagabrielle, Y. and Bodinier, J. L. (2008). Submarine reworking of exhumed subcontinental mantle rocks: field evidence from the Lherz peridotites,

French Pyrenees. *Terra Nova*, 20(1), 11–21.

Larsen, H. C., Mohn, G., Nirrengarten, M., Sun, Z., Stock, J., Jian, Z., et al. (2018). Rapid transition from continental breakup to igneous oceanic crust in the South China Sea. *Nat. Geosci.*, 11(10), 782–789.

Larvet, T., Le Pourhiet, L., Pubellier, M., and Gyomlai, T. (2023). Slab pull driven south China sea opening implies a Mesozoic proto South China Sea. *Geophys. Res. Lett.*, 50(22), article no. e2023GL105292.

Lau, K. H., Louden, K. E., Funck, T., Tucholke, B. E., Holbrook, W. S., Hopper, J. R., and Christian Larsen, H. (2006). Crustal structure across the Grand Banks—Newfoundland Basin Continental Margin—I. Results from a seismic refraction profile. *Geophys. J. Int.*, 167(1), 127–156.

Lavier, L. L. and Buck, W. R. (2002). Half graben versus large-offset low-angle normal fault: Importance of keeping cool during normal faulting. *J. Geophys. Res.: Solid Earth*, 107(B6), article no. ETG-8.

Lavier, L. L. and Manatschal, G. (2006). A mechanism to thin the continental lithosphere at magma-poor margins. *Nature*, 440(7082), 324–328.

Lavier, L. L., Roger Buck, W., and Poliakov, A. N. (1999). Self-consistent rolling-hinge model for the evolution of large-offset low-angle normal faults. *Geology*, 27(12), 1127–1130.

Le Pichon, X. and Barbier, F. (1987). Passive margin formation by low-angle faulting within the upper crust: The northern Bay of Biscay margin. *Tectonics*, 6(2), 133–150.

Le Pourhiet, L., Burov, E., and Moretti, I. (2004). Rifting through a stack of inhomogeneous thrusts (the dipping pie concept). *Tectonics*, 23(4), article no. TC4005.

Le Pourhiet, L., Chamot-Rooke, N., Delescluse, M., May, D. A., Watremez, L., and Pubellier, M. (2018). Continental break-up of the South China Sea stalled by far-field compression. *Nat. Geosci.*, 11(8), 605–609.

Le Pourhiet, L., May, D. A., Huille, L., Watremez, L., and Leroy, S. (2017). A genetic link between transform and hyper-extended margins. *Earth Planet. Sci. Lett.*, 465, 184–192.

Lecomte, E., Le Pourhiet, L., and Lacombe, O. (2012). Mechanical basis for slip along low-angle normal faults. *Geophys. Res. Lett.*, 39(3), article no. L03307.

Lecomte, E., Le Pourhiet, L., Lacombe, O., and Jolivet, L. (2011). A continuum mechanics approach to quantify brittle strain on weak faults: application to the extensional reactivation of shallow dipping discontinuities. *Geophys. J. Int.*, 184(1), 1–11.

Lemoine, M., Tricart, P., and Boillot, G. (1987). Ultramafic and gabbroic ocean floor of the Ligurian Tethys (Alps, Corsica, Apennines): In search of a genetic model. *Geology*, 15(7), 622–625.

Leroy, S., Razin, P., Autin, J., et al. (2012). From rifting to oceanic spreading in the Gulf of Aden: a synthesis. *Arab J. Geosci.*, 5, 859–901.

Liang, Y., Delescluse, M., Qiu, Y., Pubellier, M., Chamot-Rooke, N., Wang, J., et al. (2019). Décollements, detachments, and rafts in the extended crust of Dangerous Grounds, South China Sea: The role of inherited contacts. *Tectonics*, 38(6), 1863–1883.

Lister, G. S., Etheridge, M. A., and Symonds, P. A. (1986). Detachment faulting and the evolution of passive continental margins. *Geology*, 14(3), 246–250.

Lister, G. S., Etheridge, M. A., and Symonds, P. A. (1991). Detachment models for the formation of passive continental margins. *Tectonics*, 10(5), 1038–1064.

Lizarralde, D., Axen, G. J., Brown, H. E., Fletcher, J. M., González-Fernández, A., Harding, A. J., et al. (2007). Variation in styles of rifting in the Gulf of California. *Nature*, 448(7152), 466–469.

Louden, K. E. and Chian, D. (1999). The deep structure of non–volcanic rifted continental margins. *Philos. Trans. R. Soc. Lond. A*, 357(1753), 767–804.

Lu, G. and Huismans, R. S. (2022). Magmatism at passive margins: Effects of depth-dependent wide rifting and lithospheric counterflow. *J. Geophys. Res.: Solid Earth*, 127(3), article no. e2021JB023046.

Manatschal, G. (2004). New models for evolution of magma-poor rifted margins based on a review of data and concepts from West Iberia and the Alps. *Int. J. Earth Sci.*, 93, 432–466.

Manatschal, G., Froitzheim, N., Rubenach, M., and Turrin, B. D. (2001). The role of detachment faulting in the formation of an ocean-continent transition: insights from the Iberia Abyssal Plain. *Geol. Soc. Lond. Spec. Publ.*, 187(1), 405–428.

Manatschal, G. and Nievergelt, P. (1997). A continent-ocean transition recorded in the Err and Platta nappes (Eastern Switzerland). *Eclogae Geol. Helv.*,

90(1), 3–28.

Marrett, R. and Allmendinger, R. W. (1992). Amount of extension on "small" faults: An example from the Viking graben. *Geology*, 20(1), 47–50.

Masini, E., Manatschal, G., Tugend, J., Mohn, G., and Flament, J. M. (2014). The tectono-sedimentary evolution of a hyper-extended rift basin: the example of the Arzacq–Mauléon rift system (Western Pyrenees, SW France). *Int. J. Earth Sci.*, 103(6), 1569–1596.

McCarthy, A., Falloon, T. J., Sauermilch, I., Whittaker, J. M., Niida, K., and Green, D. H. (2020). Revisiting the Australian-Antarctic ocean-continent transition zone using petrological and geophysical characterization of exhumed subcontinental mantle. *Geochem. Geophys. Geosyst.*, 21(7), article no. e2020GC009040.

McKenzie, D. (1978). Some remarks on the development of sedimentary basins. *Earth Planet. Sci. Lett.*, 40(1), 25–32.

Melosh, H. J. (1990). Mechanical basis for low-angle normal faulting in the Basin and Range province. *Nature*, 343(6256), 331–335.

Mohn, G., Karner, G. D., Manatschal, G., and Johnson, C. A. (2015). Structural and stratigraphic evolution of the Iberia–Newfoundland hyper-extended rifted margin: a quantitative modelling approach. *Special Publ.*, 413(1), 53–89.

Mohn, G., Manatschal, G., Beltrando, M., Masini, E., and Kusznir, N. (2012). Necking of continental crust in magma-poor rifted margins: Evidence from the fossil Alpine Tethys margins. *Tectonics*, 31(1), article no. TC1012.

Mohn, G., Manatschal, G., Müntener, O., Beltrando, M., and Masini, E. (2010). Unravelling the interaction between tectonic and sedimentary processes during lithospheric thinning in the Alpine Tethys margins. *Int. J. Earth Sci.*, 99, 75–101.

Mohn, G., Ringenbach, J. C., Nirrengarten, M., Lei, C., McCarthy, A., and Tugend, J. (2022). Mode of continental breakup of marginal seas. *Geology*, 50(10), 1208–1213.

Morley, C. K. (2014). The widespread occurrence of low-angle normal faults in a rift setting: Review of examples from Thailand, and implications for their origin and evolution. *Earth-Sci. Rev.*, 133, 18–42.

Moulin, M., Klingelhoefer, F., Afilhado, A., Aslanian, D., Schnurle, P., Nouze, H., et al. (2015). Deep

crustal structure across a young passive margin from wide-angle and reflection seismic data (The SARDINIA Experiment)–I. Gulf of Lion's margin. *Bull. Soc. Géol. Fr.*, 186(4–5), 309–330.

Nagel, T. J. and Buck, W. R. (2007). Control of rheological stratification on rifting geometry: a symmetric model resolving the upper plate paradox. *Int. J. Earth Sci.*, 96, 1047–1057.

Naliboff, J. B., Buiter, S. J., Péron-Pinvidic, G., Osmundsen, P. T., and Tetreault, J. (2017). Complex fault interaction controls continental rifting. *Nat. Commun.*, 8(1), article no. 1179.

Neuharth, D., Brune, S., Glerum, A., Heine, C., and Welford, J. K. (2021). Formation of continental microplates through rift linkage: numerical modeling and its application to the Flemish Cap and Sao Paulo Plateau. *Geochem. Geophys. Geosyst.*, 22(4), article no. e2020GC009615.

Nielsen, T. K. and Hopper, J. R. (2004). From rift to drift: Mantle melting during continental breakup. *Geochem. Geophys. Geosyst.*, 5(7), article no. Q07003.

Nirrengarten, M., Mohn, G., Kusznir, N. J., Sapin, F., Despinois, F., Pubellier, M., et al. (2020). Extension modes and breakup processes of the southeast China-Northwest Palawan conjugate rifted margins. *Mar. Petrol. Geol.*, 113, article no. 104123.

Nonn, C., Leroy, S., Khanbari, K., and Ahmed, A. (2017). Tectono-sedimentary evolution of the eastern Gulf of Aden conjugate passive margins: Narrowness and asymmetry in oblique rifting context. *Tectonophysics*, 721, 322–348.

Odlum, M. L., Stockli, D. F., Capaldi, T. N., Thomson, K. D., Clark, J., Puigdefàbregas, C., and Fildani, A. (2019). Tectonic and sediment provenance evolution of the South Eastern Pyrenean foreland basins during rift margin inversion and orogenic uplift. *Tectonophysics*, 765, 226–248.

O'Reilly, B. M., Hauser, F., Ravaut, C., Shannon, P. M., and Readman, P. W. (2006). Crustal thinning, mantle exhumation and serpentinization in the Porcupine Basin, offshore Ireland: evidence from wide-angle seismic data. *J. Geol. Soc.*, 163(5), 775–787.

Osmundsen, P. T. and Ebbing, J. (2008). Styles of extension offshore mid-Norway and implications for mechanisms of crustal thinning at passive margins. *Tectonics*, 27(6), article no. TC6016.

Osmundsen, P. T. and Redfield, T. F. (2011). Crustal taper and topography at passive continental mar-

gins. *Terra Nova*, 23(6), 349–361.

Pérez-Gussinyé, M., Collier, J. S., Armitage, J. J., Hopper, J. R., Sun, Z., and Ranero, C. R. (2023). Towards a process-based understanding of rifted continental margins. *Nat. Rev. Earth Environ.*, 4(3), 166–184.

Pérez-Gussinyé, M. and Liu, Z. (2022). Numerical modelling of rifting: an overview, in rifted margins. In Peron-Pinvidic, G., editor, *Continental Rifted Margins 1: Definition and Methodology*, pages 265–307. Wiley/ISTE.

Pérez-Gussinyé, M. and Reston, T. J. (2001). Rheological evolution during extension at nonvolcanic rifted margins: Onset of serpentinization and development of detachments leading to continental breakup. *J. Geophys. Res.: Solid Earth*, 106(B3), 3961–3975.

Péron-Pinvidic, G. and Manatschal, G. (2010). From microcontinents to extensional allochthons: witnesses of how continents rift and break apart? *Pet. Geosci.*, 16(3), 189–197.

Péron-Pinvidic, G., Manatschal, G., Masini, E., Sutra, E., Flament, J. M., Haupert, I., and Unternehr, P. (2017). Unravelling the along-strike variability of the Angola–Gabon rifted margin: a mapping approach. *Geol. Soc. Lond. Spec. Publ.*, 438(1), 49–76.

Péron-Pinvidic, G., Manatschal, G., Minshull, T. A., and Sawyer, D. S. (2007). Tectonosedimentary evolution of the deep Iberia-Newfoundland margins: Evidence for a complex breakup history. *Tectonics*, 26(2), article no. TC2011.

Peron-Pinvidic, G., Manatschal, G., and Osmundsen, P. T. (2013). Structural comparison of archetypal Atlantic rifted margins: A review of observations and concepts. *Mar. Pet. Geol.*, 43, 21–47.

Petri, B., Duretz, T., Mohn, G., Schmalholz, S. M., Karner, G. D., and Müntener, O. (2019). Thinning mechanisms of heterogeneous continental lithosphere. *Earth Planet. Sci. Lett.*, 512, 147–162.

Pichot, T., Delescluse, M., Chamot-Rooke, N., Pubellier, M., Qiu, Y., Meresse, F., et al. (2014). Deep crustal structure of the conjugate margins of the SW South China Sea from wide-angle refraction seismic data. *Mar. Petrol. Geol.*, 58, 627–643.

Popov, A. A. and Sobolev, S. V. (2008). SLIM3D: A tool for three-dimensional thermomechanical modeling of lithospheric deformation with elasto-visco-plastic rheology. *Phys. Earth Planet. Inter.*, 171(1–4), 55–75. ISSN 0031-9201.

Précigout, J., Gueydan, F., Garrido, C. J., Cogné, N.,

and Booth-Rea, G. (2013). Deformation and exhumation of the Ronda peridotite (Spain). *Tectonics*, 32(4), 1011–1025.

Ranero, C. R. and Pérez-Gussinyé, M. (2010). Sequential faulting explains the asymmetry and extension discrepancy of conjugate margins. *Nature*, 468(7321), 294–299.

Räss, L., Duretz, T., Podladchikov, Y. Y., and Schmalholz, S. M. (2017). M2Di: Concise and efficient MATLAB 2-D Stokes solvers using theFinite Difference Method. *Geochem. Geophys. Geosyst.*, 18, 755–768.

Reston, T. (2007a). Extension discrepancy at North Atlantic nonvolcanic rifted margins: Depth-dependent stretching or unrecognized faulting? *Geology*, 35(4), 367–370.

Reston, T. and McDermott, K. (2014). An assessment of the cause of the 'extension discrepancy' with reference to the west Galicia margin. *Basin Res.*, 26(1), 135–153.

Reston, T. J. (1988). Evidence for shear zones in the lower crust offshore Britain. *Tectonics*, 7(5), 929–945.

Reston, T. J. (2005). Polyphase faulting during the development of the west Galicia rifted margin. *Earth Planet. Sci. Lett.*, 237(3–4), 561–576.

Reston, T. J. (2007b). The formation of non-volcanic rifted margins by the progressive extension of the lithosphere: the example of the West Iberian margin. *Geol. Soc. Lond. Spec. Publ.*, 282(1), 77–110.

Reston, T. J. (2009). The structure, evolution and symmetry of the magma-poor rifted margins of the North and Central Atlantic: A synthesis. *Tectonophysics*, 468(1–4), 6–27.

Ribes, C., Ghienne, J. F., Manatschal, G., Dall'Asta, N., Stockli, D. F., Galster, F., et al. (2020). The Grès Singuliers of the Mont Blanc region (France and Switzerland): stratigraphic response to rifting and crustal necking in the Alpine Tethys. *Int. J. Earth Sci.*, 109, 2325–2352.

Rigo, A., Lyon-Caen, H., Armijo, R., Deschamps, A., Hatzfeld, D., Makropoulos, K., et al. (1996). A microseismic study in the western part of the Gulf of Corinth (Greece): implications for large-scale normal faulting mechanisms. *Geophys. J. Int.*, 126(3), 663–688.

Roberts, A. M., Kusznir, N. J., Yielding, G., and Styles, P. (1998). 2D flexural backstripping of extensional basins; the need for a sideways glance. *Pet. Geosci.*,

4(4), 327–338.

Royden, L. and Keen, C. E. (1980). Rifting process and thermal evolution of the continental margin of eastern Canada determined from subsidence curves. *Earth Planet. Sci. Lett.*, 51(2), 343–361.

Ruppel, C. (1995). Extensional processes in continental lithosphere. *J. Geophys. Res.: Solid Earth*, 100(B12), 24187–24215.

Sapin, F., Ringenbach, J. C., and Clerc, C. (2021). Rifted margins classification and forcing parameters. *Sci. Rep.*, 11(1), article no. 8199.

Sawyer, D. S., Whitmarsh, R. B., Klaus, A., and Party, S. S. (1994). *Proceedings of the ODP, Init. Repts., 149*. Ocean Drilling Program, College Station, Texas.

Schmalholz, S. M. and Mancktelow, N. S. (2016). Folding and necking across the scales: a review of theoretical and experimental results and their applications. *Solid Earth*, 7(5), 1417–1465.

Sclater, J. G. and Christie, P. A. (1980). Continental stretching: An explanation of the post-mid-Cretaceous subsidence of the central North Sea basin. *J. Geophys. Res.: Solid Earth*, 85(B7), 3711–3739.

Simonetti, M., Langone, A., Corvò, S., and Bonazzi, M. (2021). Triassic-jurassic rift-related deformation and temperature-time evolution of the fossil adriatic margin: a review from Ossola and Strona di Omegna valleys (Ivrea-Verbano zone). *Ofioliti*, 46(2), 151–165.

Steckler, M. S., Berthelot, F., Lyberis, N., and Le Pichon, X. (1988). Subsidence in the Gulf of Suez: implications for rifting and plate kinematics. *Tectonophysics*, 153(1–4), 249–270.

Sutra, E., Manatschal, G., Mohn, G., and Unternehr, P. (2013). Quantification and restoration of extensional deformation along the Western Iberia and Newfoundland rifted margins. *Geochem. Geophys. Geosyst.*, 14(8), 2575–2597.

Svartman Dias, A. E., Hayman, N. W., and Lavier, L. L. (2016). Thinning factor distributions viewed through numerical models of continental extension. *Tectonics*, 35(12), 3050–3069.

Svartman Dias, A. E., Lavier, L. L., and Hayman, N. W. (2015). Conjugate rifted margins width and asymmetry: The interplay between lithospheric strength and thermomechanical processes. *J. Geophys. Res.: Solid Earth*, 120(12), 8672–8700.

Taylor, B. and Huchon, P. (2002). Active continen-

tal extension in the western Woodlark Basin: A synthesis of leg 180 results. In *Proceedings of the Ocean Drilling Program, 180 Scientific Results*. Ocean Drilling Program, College Station, Texas.

Tetreault, J. L. and Buiter, S. J. H. (2018). The influence of extension rate and crustal rheology on the evolution of passive margins from rifting to breakup. *Tectonophysics*, 746, 155–172.

Thinon, I., Matias, L., Réhault, J. P., Hirn, A., Fidalgo-González, L., and Avedik, F. (2003). Deep structure of the Armorican Basin (Bay of Biscay): a review of Norgasis seismic reflection and refraction data. *J. Geol. Soc.*, 160(1), 99–116.

Tirel, C., Brun, J. P., and Burov, E. (2008). Dynamics and structural development of metamorphic core complexes. *J. Geophys. Res.: Solid Earth*, 113(B4), article no. B04403.

Tugend, J., Gillard, M., Manatschal, G., Nirrengarten, M., Harkin, C., Epin, M. E., et al. (2020). Reappraisal of the magma-rich versus magma-poor rifted margin archetypes. *Geol. Soc. Lond. Spec. Publ.*, 476(1), 23–47.

Tugend, J., Manatschal, G., Kusznir, N. J., and Masini, E. (2015). Characterizing and identifying structural domains at rifted continental margins: application to the Bay of Biscay margins and its Western Pyrenean fossil remnants. *Geol. Soc. Lond. Spec. Publ.*, 413(1), 171–203.

Tugend, J., Manatschal, G., Kusznir, N. J., Masini, E., Mohn, G., and Thinon, I. (2014). Formation and deformation of hyperextended rift systems: Insights from rift domain mapping in the Bay of Biscay-Pyrenees. *Tectonics*, 33(7), 1239–1276.

Welford, J. K., Smith, J. A., Hall, J., Deemer, S., Srivastava, S. P., and Sibuet, J. C. (2010). Structure and rifting evolution of the northern Newfoundland Basin from Erable multichannel seismic reflection profiles across the southeastern margin of Flemish Cap. *Geophys. J. Int.*, 180(3), 976–998.

Wernicke, B. (1981). Low-angle normal faults in the Basin and Range Province: nappe tectonics in an extending orogen. *Nature*, 291(5817), 645–648.

Wernicke, B. (1995). Low-angle normal faults and seismicity: A review. *J. Geophys. Res.*, 100(B10), 20159–20174.

Wernicke, B. and Axen, G. J. (1988). On the role of isostasy in the evolution of normal fault systems. *Geology*, 16(9), 848–851.

White, R. and McKenzie, D. (1989). Magmatism at

rift zones: the generation of volcanic continental margins and flood basalts. *J. Geophys. Res.: Solid Earth*, 94(B6), 7685–7729.

White, R. S. and Smith, L. K. (2009). Crustal structure of the Hatton and the conjugate east Greenland rifted volcanic continental margins, NE Atlantic. *J. Geophys. Res.: Solid Earth*, 114(B2), article no. B02305.

Whitmarsh, R. B., Manatschal, G., and Minshull, T. A. (2001). Evolution of magma-poor continental margins from rifting to seafloor spreading. *Nature*, 413(6852), 150–154.

Whitney, D. L., Teyssier, C., Rey, P., and Buck, W. R. (2013). Continental and oceanic core complexes. *Bulletin*, 125(3–4), 273–298.

Zelt, C. A., Sain, K., Naumenko, J. V., and Sawyer, D. S. (2003). Assessment of crustal velocity models using seismic refraction and reflection tomography. *Geophys. J. Int.*, 153(3), 609–626.